

# Emerging Planar Nanostructures Involving Both Local and Nonlocal Modes

Ruoheng Chai, Qi Liu, Wenwei Liu,\* Zhancheng Li, Hua Cheng,\* Jianguo Tian, and Shuqi Chen\*

Cite This: <https://doi.org/10.1021/acsphotonics.2c01534>

Read Online

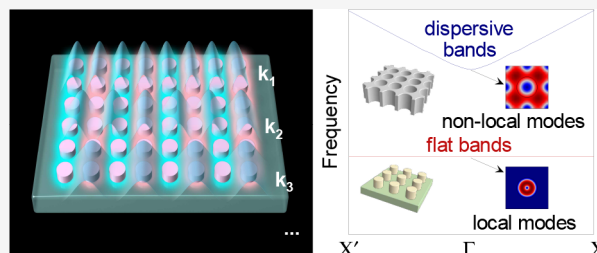
ACCESS |

Metrics &amp; More

Article Recommendations

**ABSTRACT:** With the capabilities to localize light at the subwavelength scale and flexibly control the full dimensions of electromagnetic fields, planar optical artificial nanostructures have been widely explored to innovate next-generation multifunctional compact photonic devices in recent decades. To further improve the efficiency, quality ( $Q$ ) factors, and design degrees of freedom of photonic devices, recent research advances have brought in comprehensive consideration of both local and nonlocal modes in nanostructures with blurred distinctions between metasurfaces and photonic crystals. In this Perspective, we review the recent progress in planar nanophotonics involving localized resonances, nonlocal modes, and their couplings. Many intriguing physical effects correlated to local and/or nonlocal modes and the corresponding applications are reviewed, as well as large-area optimization strategies to directly simulate local and nonlocal optical responses. We also summarize several current challenges and foresee various future directions of the attractive field.

**KEYWORDS:** photonic crystals, metasurfaces, bound states in the continuum, mode couplings, optimization strategies



## INTRODUCTION

Optical artificial nanostructures can achieve subwavelength localization of light by various resonances, such as localized surface plasmon resonances (LSPRs) in metallic nanoparticles,<sup>1</sup> Bragg resonances in photonic crystals,<sup>2</sup> and Mie resonances in dielectric resonators.<sup>3–6</sup> These resonances provide unprecedented light–matter interaction strengths, which can be used to enhance many optical effects, including optical force, Raman scattering, lasing, and optical harmonic generation.<sup>7–11</sup> In recent years, planar optical artificial nanostructures have received a substantial amount of attention from researchers owing to their feasibility in fabrication, efficient light–matter interaction, and flexible manipulation of electromagnetic fields.<sup>12</sup> Planar optical artificial nanostructures can be classified into two main categories: two-dimensional (2D) photonic crystals and metasurfaces. Photonic crystals support extended nonlocal modes (typically Bloch modes or waveguide modes propagating along the array directions) and generally achieve in-plane light confinement by defect modes inside the photonic band gap.<sup>13</sup> Here we clarify that the “nonlocal modes” refer to the optical responses of individual meta-atoms, which are dictated by fields or scatters at distant locations, including Bloch modes, waveguide modes, and various bulk modes with mode volumes far larger than the wavelength. The nonlocal modes in periodic structures are generally analyzed by band theory and depicted by wave vectors instead of positions.<sup>2</sup> Photonic crystals are excellent

media to trap spatial light but lack effective methods to achieve multidimensional manipulation of optical fields.

On the other hand, metasurfaces exploit local modes that are not sensitive to the differences among elementary resonators empowering flexible manipulation of the amplitudes, phases, and polarizations of light by subwavelength spatial arrangements of nanoresonators. The local modes are functions of certain locations, highlighting the independence of optical responses at a single meta-atom or metamolecule from neighboring unit cells, including LSPRs, Mie resonances, and defect modes with a subwavelength mode volume and negligible neighboring interactions. For example, metasurfaces usually load desirable phase distributions by Pancharatnam–Berry (PB) phases<sup>14</sup> or resonant phases<sup>15</sup> of unit cells with periodic boundary conditions. Then the various unit cells are regarded as building blocks to construct the phase distributions in a discretized way (this process should satisfy the Nyquist sampling theorem). However, this design strategy has several natural drawbacks: First, metallic nanostructures suffer from intrinsic ohmic loss in the visible and infrared bands<sup>16</sup> and thus

**Special Issue:** Photonics in China

**Received:** September 30, 2022

**Revised:** January 8, 2023

**Accepted:** January 9, 2023

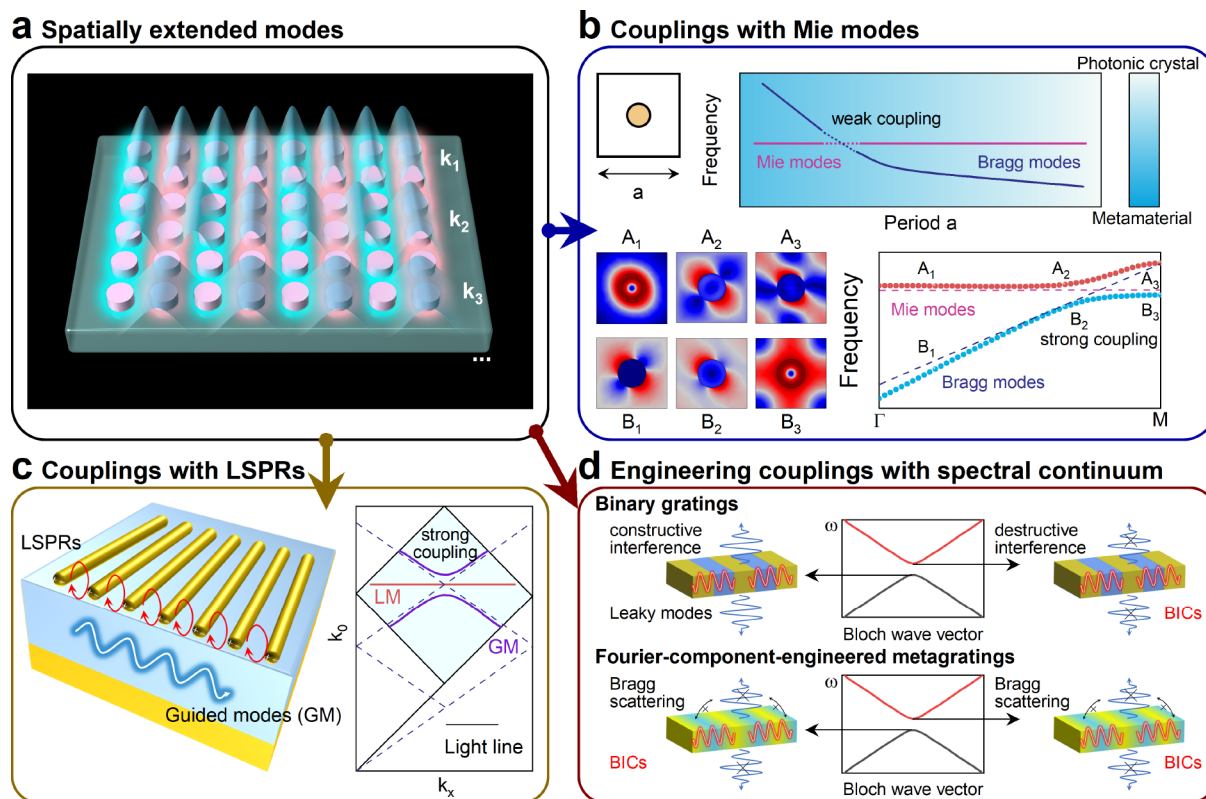


**Figure 1.** Nonlocal modes and their couplings with other modes or waves. (a) Schematic of nonlocal modes with different momentum supported by periodic artificial nanostructures. (b) Weak couplings between nonlocal Bragg modes and localized Mie modes, in which metamaterials and photonic crystals are distinguished by the Bragg and Mie band gaps. Not only weak couplings but also strong couplings between Bragg modes and Mie modes can be realized by engineering the system parameters (for example, periods and wave vectors, respectively). Mode exchange and avoided crossing can be observed in the strong coupling regime. (c) Couplings between nonlocal guided modes and localized surface plasma resonance (LSPR) modes. (d) Conventional BICs in periodic nanostructures such as binary gratings originate from the destructive interference between a pair of counter-propagating guided waves in momentum space, while constructive interference leads to the formation of leaky modes. Fourier-component-engineered metagratings can support BICs at both upper and lower bands by eliminating specific Bragg scattering processes.

the quality ( $Q$ ) factors<sup>17</sup> are limited to a typical value of 10, even though the light localizations by metallic nanoparticles can reach a deep-subwavelength scale (the localization assumption of unit cells is valid). Second, subwavelength nanostructures made of dielectric materials (low intrinsic loss) support Mie resonances that have larger mode volumes and the collective lattice resonances (nonlocal modes) can be easily excited.<sup>18,19</sup> Some of the coupled modes oscillating in nondiffractive metasurfaces possess high  $Q$  factors, but the neighboring interactions can hardly be neglected, which means that the local optical response of the meta-atoms in the supercells cannot be simply determined by the elementary nanoresonators. As a result, the non-negligible neighboring interactions lead to low efficiency if one constructs metasurfaces according to the conventional strategy. Third, an ultrahigh refractive index material is essential for Mie resonators to achieve ideal spatial and temporal confinements of light.<sup>20</sup> However, ultrahigh refractive index materials are rare in the visible and infrared bands since the refractive index of natural dielectric materials is lower with higher frequencies. For example, the refractive index of water can reach 9 in the microwave band but decrease to approximately 1.4 in the visible and infrared bands. In brief, the simultaneous realization of high- $Q$ , highly efficient, and multidimensional light manipulation is very challenging.

Fortunately, an emerging design strategy with blurred distinctions between photonic crystals and metasurfaces is

expected to solve the long-standing problem.<sup>21–26</sup> Considering both the local and nonlocal optical responses of nanostructures, one can potentially achieve both flexible and high- $Q$  light manipulations enabled by subwavelength structural designs and nonlocal collective resonances, respectively. In the past decade, a concept that originates from quantum physics named bound states in the continuum (BICs)<sup>27,28</sup> has been introduced in photonic crystals and metasurfaces, revealing that these optical artificial nanostructures can support nonlocal modes with infinite  $Q$  factors at some discrete  $k$  points, as a result of destructive interference.<sup>29</sup> Being embedded in the radiative continuum, BICs can be selectively out-coupled to the spectral continuum with specific narrow-bands, amplitudes, phases, and polarization states by elaborate structural perturbations.<sup>22,30</sup> The structural perturbations transform ideal BICs into quasi-BICs and the behavior of  $Q$  factors is typically inverse exponential for the dimensionless perturbation parameters.<sup>31</sup> Emergent optical nanostructures apply subwavelength perturbations on the unit cells of photonic crystals or waveguides to locally manipulate the leaky waves. However, it is difficult to eliminate the neighboring couplings, leading to a lower efficiency. One direct solution is seeking compensation. For example, the rippled PB phases that result from the neighboring couplings can be compensated by resonant phases through tiny geometric adjustments of meta-atoms.<sup>24–26,32</sup> However, this approach still focuses on the local construction of metasurfaces and relies on time-consuming simulations to

build structural libraries of meta-atoms, especially for nonlinear metasurfaces. The high demands on the nanostructure geometry limit its efficiency and practical applications as well. Another idea is large-area simulation or optimization, which directly counts the neighboring interactions within the large-area nanostructures and neglects the dispensable neighboring effects at the boundary.<sup>33</sup> This approach regards large-area meta-atoms as unity, which means that researchers require a targeted design of the overall optical potential (or impedance) and/or assisted optimization algorithms. Large-area optimizations exploit the global effects to design optical functionalities, which are more robust to disorders in nanofabrications and are expected to develop multifunctional, well-performing, highly efficient optical devices with ultrahigh  $Q$  factors.<sup>34</sup>

In this Perspective, we emphasize the emerging concepts of artificial nanostructures involving both local and nonlocal modes. We review the key advances of this promising field, discussing the physics of the correlated optical effects and their applications. We concentrate on nonlocal modes and their couplings to local resonances, guided modes, and spectral continuums. Particularly, we touch on the interference between counter-propagating guided modes and couplings with localized surface plasma resonances (LSPRs), Mie resonances, and free-space radiative waves. In addition, we summarized the current tendency to consider and utilize the neighboring couplings in meta-atoms, including engineering the Fourier components of the dielectric functions and algorithm-supported large-scale optimizations. Finally, an outlook expressing our viewpoints on challenges and future directions in artificial nanostructures involving both local and nonlocal modes is presented.

## ■ NOVEL OPTICAL EFFECTS

Metasurfaces are planar ensembles of nanoresonators or meta-atoms that can flexibly control the frequency, amplitude, phase, wavefront, and even coherence of light.<sup>12,35–39</sup> Compared to three-dimensional metamaterials, metasurfaces can not only dramatically reduce the optical loss and fabrication complexity but also provide the flexibility to efficiently manipulate various degrees of freedom of light and thus have received tremendous attention from researchers. Traditionally, metasurfaces with subwavelength elementary units control the electromagnetic fields through an independent spatial arrangement of meta-atoms, which have been widely applied to many fabulous implications, such as metalenses, holography, optical vortex beams, lasing, and nonlinear harmonics.<sup>39–43</sup> In contrast to the conventional metasurfaces exploiting local resonances, the nonlocal artificial nanostructures, such as metagratings and photonic crystal slabs, can support high- $Q$  guided mode resonances that transversely extend over a large area of the nanostructures.<sup>21,44</sup> Very recently, a novel design route has been suggested to effectively realize functional and compact photonic devices with sharp spectral responses combining the concepts of nonlocal modes and locally designed metasurfaces.<sup>22</sup> In addition, numerous intriguing optical phenomena have been uncovered based on this newly developed strategy.<sup>45–47</sup>

We first summarize the optical coupling relations of nonlocal modes in planar artificial nanostructures in Figure 1, including couplings with the local resonances (Mie resonances for dielectric nanostructures and LSPRs for metallic materials) and with themselves via radiation continuum by Bragg scatterings

(typical BICs). The behaviors of optical modes in periodic or quasi-periodic nanostructures can be effectively analyzed by band theory with different Bloch wave vectors  $k$  as long as neighboring interactions exist, as shown in Figure 1a. Dielectric artificial nanostructures can support both nonlocal Bragg modes and localized Mie resonances, and the interactions or dominant modes can be engineered by the system parameters.<sup>48</sup> For example, in a 2D photonic crystal consisting of dielectric nanorods, the nonlocal Bragg modes and the localized Mie modes can couple with each other in the weak or strong coupling regimes, as illustrated in Figure 1b. In the weak coupling regime, the Bragg and Mie modes cross at specific parameter coordinates (for example, period  $a$ ) owing to the different dispersion relations for the system parameters. Researchers usually concentrate on several fundamental modes with lower frequencies because the low-frequency modes have no diffractive loss. The dominant modes in the low-frequency region shift from Mie modes to Bragg modes when one tailors the period of the 2D nanorod array, showing a phase transition from metamaterials to photonic crystals. The resultant crossing regions of the fundamental Mie and Bragg modes show blurred boundaries between metamaterials and photonic crystals. On the other hand, strong couplings in parameter space result in avoided crossings and hybridization of the Mie modes and Bragg modes, as shown in the lower panels in Figure 1b. Taking the momentum space as an example, the dispersive Mie bands maintain their characteristic of near-field localization around the  $\Gamma$  point, but their electromagnetic energy gradually expands to the whole unit cells with the wave vector shifting from the  $\Gamma$  point to the  $M$  point. Indeed, both local and nonlocal optical responses can coexist within the same dielectric nanostructure, and the dominant effect or their superposition depends on the system parameters.<sup>49</sup>

We now briefly discuss metallic metamaterials that support local modes such as LSPRs on a deep-subwavelength scale. LSPRs are collective oscillations of the conduction electrons and the irradiating light on the surface of a nanoparticle with a size comparable to or smaller than the incident wavelength.<sup>1</sup> In metallic or semiconductor nanostructures, LSPRs can couple with nonlocal modes as well.<sup>50–52</sup> The common configurations are metallic nanoparticle arrays with covering or underlying thin dielectric layers to take advantage of the near-field couplings between LSPRs and guided modes, as depicted in Figure 1c. The guided modes are highly dispersive with in-plane momentum  $k_x$ , while the local modes of LSPRs are flat bands due to the absence of interactions between neighboring plasmonic resonators. Interestingly, the neighboring interactions can be introduced by an indirect route—via nonlocal guided modes.<sup>53</sup> Strong or weak couplings between LSPRs and guided modes can be realized by tailoring the system parameters such as the height or period of the metallic meta-atoms. Underpinned by these rich coupling mechanisms, the complex frequency and the spatial properties of the eigenmodes can be engineered at will, which inspires many novel effects, such as exceptional points (EPs),<sup>53</sup> BICs,<sup>54–56</sup> and unidirectional lossless surface plasma propagations.<sup>57</sup>

BICs are bound states embedded in but orthogonal to the radiation continuum, ideally possessing infinite radiative  $Q$  factors.<sup>28,58</sup> The novel photonic bound states originate from the destructive interference of the counter-propagating guided mode resonances in the strong coupling regime,<sup>59</sup> as illustrated in Figure 1d. At the same time, the other guided mode is leakier due to constructive interference. In addition, the

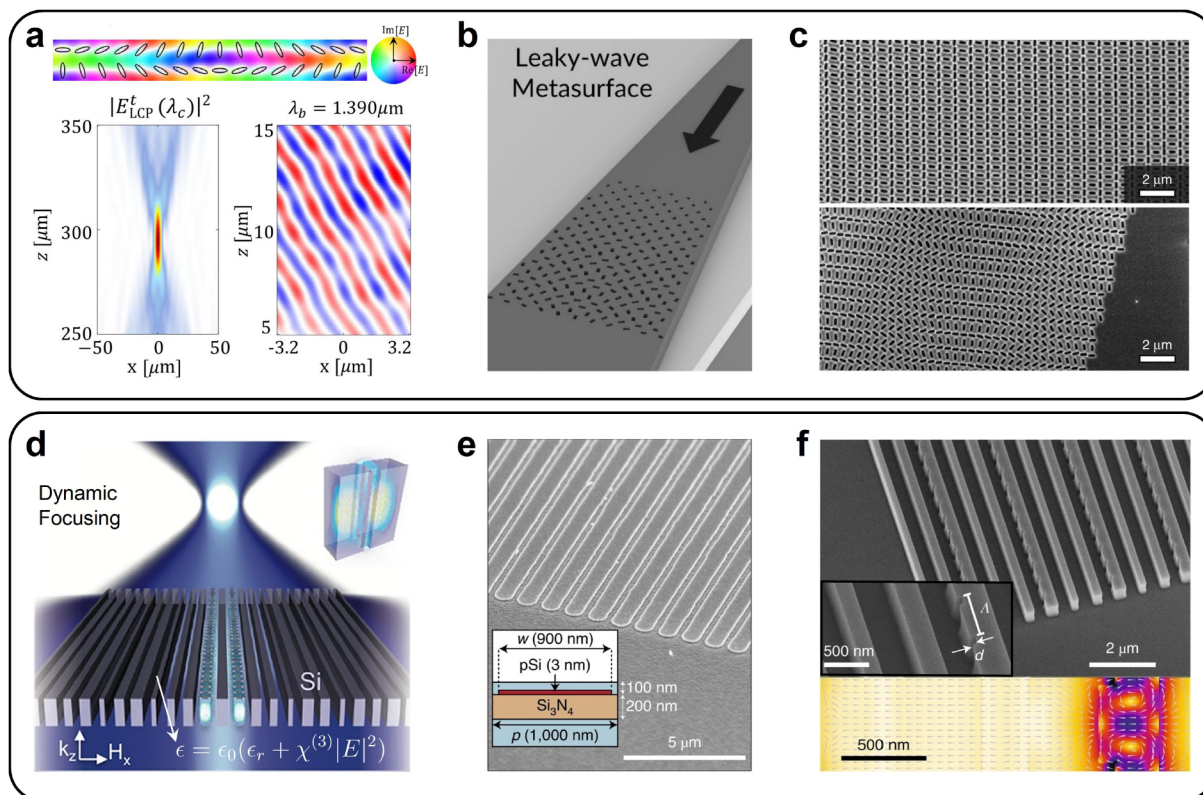


**Figure 2.** Perturbative nonlocal metasurfaces and metagratings. (a) Wavefront shaping and focusing based on quasi-BIC metasurfaces.<sup>21</sup> (b) Schematic of on-chip quasi-BIC metasurfaces achieving full-dimensional manipulations (amplitudes, phases, and polarizations) of leaky waves.<sup>22</sup> (c) SEM image of multifunctional few-layer metasurfaces exploiting multiperturbations on nonlocal modes.<sup>23</sup> (d) Dynamic focusing by perturbative metagratings composed of photorefractive silicon nanolines.<sup>72</sup> (e) SEM image of superthin high-Q metagratings with independent diffraction efficiency across different wavelength bands.<sup>44</sup> (f) High-Q phase gradient metagratings based on perturbations on guided modes.<sup>73</sup> (a) Reprinted with permission from ref 21. Copyright 2020 American Physical Society. (b) Reprinted under the terms of Creative Commons license (<https://creativecommons.org/licenses/by/4.0/>) from ref 22. Copyright 2022 the Authors. (c) Reprinted under the terms of Creative Commons license (<https://creativecommons.org/licenses/by/4.0/>) from ref 23. Copyright 2022 the Authors, published by Springer Nature. (d) Reprinted with permission from ref 72. Copyright 2020 American Chemical Society. (e) Reprinted with permission from ref 44. Copyright 2021 Nature Publishing Group. (f) Reprinted with permission from ref 73. Copyright 2020 Nature Publishing Group.

symmetry and topological properties of BICs are revealed at both highly symmetric and general points in momentum space.<sup>31,60–64</sup> Very recently, a novel class of BICs has been achieved by engineering Bragg scattering processes in metagratings, which can be tailored by the Fourier components of the nanostructures' dielectric functions.<sup>65</sup> In contrast to the conventional BICs that are located at discrete points in the momentum space and show a sharp decline in the  $Q$  factors when deviating from BIC points, the metagratings with meticulously engineered Fourier components support BICs at arbitrary bands in a considerable range centered on the highly symmetric points (for example,  $\Gamma$  points). The Fourier-engineering strategy directly manipulates the coupling strengths between nonlocal guided modes and the free-space radiation continuum,<sup>66–68</sup> inspiring  $k$ -space engineering of the metasurfaces involving nonlocal modes.<sup>69</sup> The Fourier-component-engineered BICs are angular robust, naturally multiband, and independent of geometric parameters, making it a promising mechanism to realize many fascinating applications such as high numerical aperture (NA) filters, high harmonic generation by tightly focused pumping, and low threshold lasers.

To experimentally demonstrate BICs, it is necessary to transform ideal BICs into resonant modes with ultrahigh but finite  $Q$  factors (quasi-BICs). High- $Q$  metasurfaces based on

BICs are typically realized by structural and symmetrical perturbations in periodic planar nanostructures, with an inverse exponential dependence on the asymmetry parameters<sup>70</sup> (the power depends on the order of BICs<sup>62</sup>). However, conventional strategies that locally manipulate the amplitudes and phases of light are not suitable for quasi-BIC metasurfaces because the high- $Q$  characteristic originates from the couplings of the nonlocal Bragg resonances. In addition, the near-field couplings can hardly be neglected because these BICs are protected by the symmetry of the near-field distributions.<sup>71</sup>

Based on the aforementioned concept of BICs, an emergent strategy was proposed and proved to be effective to manipulate light with various degrees of freedom and simultaneously maintain high  $Q$  factors, in which deliberate perturbations were introduced on the bound states inside the waveguides to cancel out the neighboring interactions. Figure 2 shows metasurfaces with perturbations on the nonlocal modes, which introduce weak couplings to the diffraction channels. Figure 2a–c illustrates the nondiffractive perturbative guided mode metasurfaces,<sup>21–23</sup> which can be regarded as perturbations on BIC modes supported by the original photonic slabs, a kind of quasi-BIC.<sup>24,25,32</sup> For example, in Figure 2a, the original air holes of the photonic slabs are perturbed from circular to elliptical with varying orientation angles to generate phase gradients (PB phase). The authors proposed using a pair of

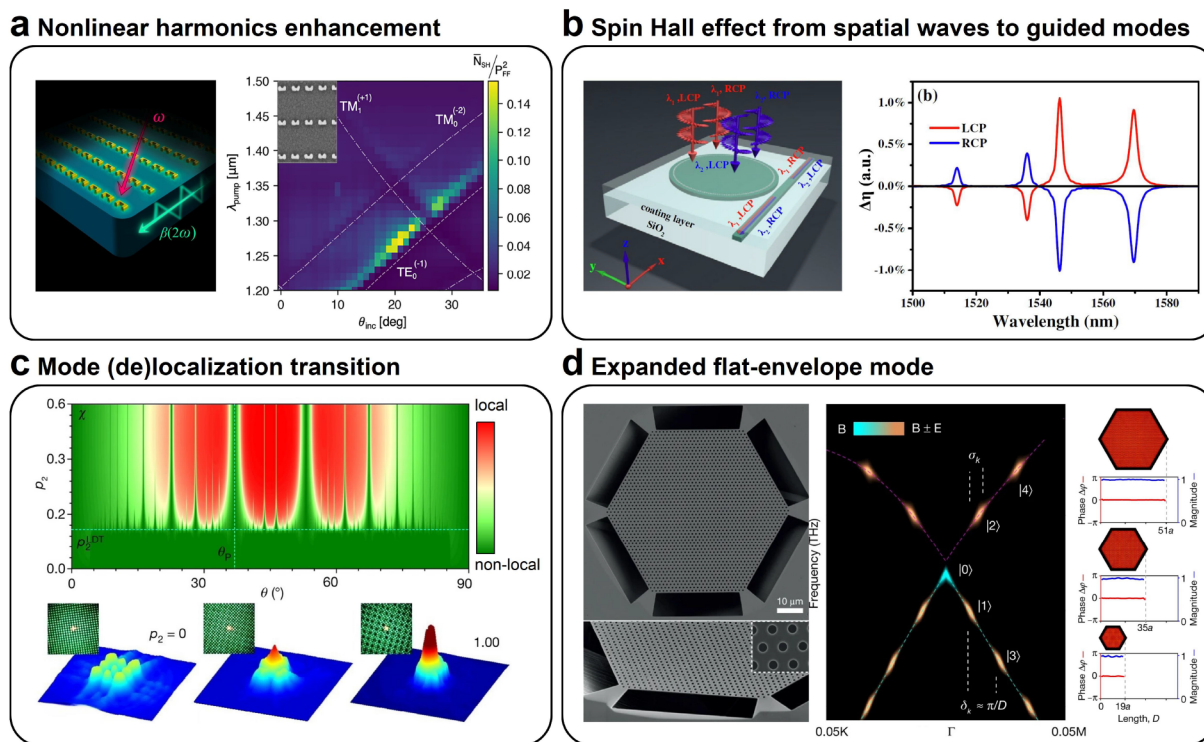


**Figure 3.** Novel optical effects in artificial nanostructures involving local and nonlocal modes. (a) Illustration of the second harmonic enhancements from a gold split-ring-resonator metasurface coupled with guided modes. Measured transmitted second harmonics versus the incident angle and the wavelength of the fundamental waves. The dispersion of the second harmonics roughly follows the guided TE mode.<sup>74</sup> (b) Schematic of the on-chip photonic spin Hall effect, in which the artificial nanostructures on the microcavity selectively couple the spatial light into the guided modes with different propagation directions. Coupling efficiency difference between incident optical waves with opposite spins.<sup>75</sup> (c) Transition of spatially localized mode and nonlocal mode by engineering the magic angle and the modulation depths of two sublattices in a Moiré lattice.<sup>45</sup> (d) SEM images of the open Dirac optical cavity made of InGaAsP multiple quantum wells. The finite open photonic crystal cavity still maintains the Dirac dispersion. Pure nondegenerate mode B is located at the apex of the Dirac cone, and it expands the whole cavity with a flat envelope despite cavity scales.<sup>46</sup> (a) Reprinted under the terms of Creative Commons license (<https://creativecommons.org/licenses/by/4.0/>) from ref 74. Copyright 2022 the Authors, published by American Chemical Society. (b) Reprinted with permission from ref 75. Copyright 2021 The Optical Society. (c) Reprinted with permission from ref 45. Copyright 2020 Nature Publishing Group. (d) Reprinted with permission from ref 46. Copyright 2022 Nature Publishing Group.

orthogonal elliptical holes as a rotation unit to cancel out the neighboring interactions.<sup>21</sup> Based on the perturbative nonlocal metasurfaces, the phase of the circularly polarized light can be locally engineered with a high and roughly invariant efficiency. Furthermore, the authors demonstrated resultant functionalities, including focusing, abnormal reflection and transmission, and multiband abnormal refractions by utilizing the perturbed nonlocal metasurfaces. In addition, the polarization conversion efficiency can be further enlarged to approximately 1 by few-layer metasurfaces with subtle scales among unit cells in the supercell.<sup>26</sup> This strategy can be extended to waveguides as well, as shown in Figure 2b.<sup>22</sup> Full degrees of freedom including amplitude, phase, and polarization states of light can be further manipulated by tailoring the geometric parameters of the perturbed meta-atoms. Accordingly, on-chip beam convergence and holography were achieved.<sup>22</sup> Figure 2c shows the SEM images of the multilayer perturbative nonlocal metasurfaces, by which multifunctional resonant focusing and abnormal refraction were experimentally observed, and applications of augmented reality were further conceptually demonstrated.<sup>23</sup>

In addition to perturbative nonlocal metasurfaces, diffractive metagratings are an alternative to achieve efficient narrow-band optical field manipulations. Figure 2d–e illustrates representative works of diffractive metagratings that apply nanoscale

defects in homogeneous waveguides to construct supercells and introduce minimal couplings to the diffraction channels.<sup>44,72,73</sup> The periodic metasurfaces consist of multiple equally spaced nanobars with slightly different widths and subtle perturbations, as illustrated in Figure 2d. The nanostructure can be constructed in two steps to realize phase gradients and high-Q resonances. The first step is a width perturbation of the nanobar meta-atoms, which provides in-plane phase gradients, enlarges the meta-atoms to supercells, and folds the bands under the light cone to the upper spectral continuum (BICs). Next, the nanonotch defects are introduced, leading to weak couplings to the free-space diffraction channels, realizing transitions from BICs to quasi-BICs (modes shown in Figure 2d).<sup>72</sup> The high-Q gradient metasurfaces are constructed in such a way that the phase modulations are not correlated with the high Q factors resulting from the nonlocal guided modes. Utilizing the perturbative metasurfaces made of nonlinear Kerr materials, the authors further demonstrated a dynamic focusing metalens controlled by the pump light intensity.<sup>72</sup> Following the theoretical design, an experimental demonstration of narrow-band beam steering metagratings was reported with a measured Q factor of approximately 8200.<sup>73</sup> The SEM image of the typical nanostructure and the resonant mode distributions are shown in Figure 2f. Furthermore, slow-light beam steering and beam splitting were experimentally

achieved by harnessing the interplay between nonlocal guided waves and the gradient phase profiles of the perturbative metagratings.<sup>73</sup> In addition to nanonotch defects, an atomically thin perturbative metasurface was reported in recent years, as shown in Figure 2e.<sup>44</sup> The 7 nm thick polycrystalline silicon (pSi) layer can be regarded as periodic perturbations on the original guided waves that are trapped beneath 200 nm thick silicon nitride slabs. The authors achieved decoupling between visible and near-infrared resonant diffractions by leveraging the absorption difference of pSi between the visible and near-infrared bands.<sup>44</sup> In the visible band, the thin pSi layer absorbs more light energy so that the light energy in high-order guided modes dissipates before it decouples to free space, leading to a low first-order diffraction efficiency and a higher zero-order transmittance. In the near-infrared bands, the pSi layer acts as a high-*Q* grating coupler connecting spatial waves to the guided modes, showing resultant narrowband resonant diffractions. Taking advantage of the wavelength-decoupled diffraction, an eye-tracking glass without intense rainbows was demonstrated.<sup>44</sup>

In addition to BICs, there are other prominent advances and nontrivial optical effects involving local and nonlocal modes, as shown in Figure 3. Consistently, nonlinear harmonic excitations are research hotspots in nanophotonics due to the extreme enhancement of nonlinear efficiency enabled by the ability to spatially and temporally trap electromagnetic energies.<sup>39,70,76–80</sup> Benefiting from the strengthened light–matter interactions, various applications have been demonstrated based on local and nonlocal modes, ranging from nonlinear coding,<sup>81</sup> harmonic optical vortices,<sup>82</sup> multiplexing,<sup>42</sup> and holography<sup>83</sup> to high-order harmonic generation,<sup>84</sup> hybrid metasurfaces with 2D materials,<sup>85</sup> and asymmetric nonlinear grayscale imaging.<sup>86</sup> In the earlier studies of nonlinear metasurfaces, it was suggested that nonlinear signals can be prominently enhanced when satisfying resonant conditions at both fundamental and harmonic frequencies.<sup>87</sup> Very recently, a hybrid metasurface composed of gold split-ring resonators (SRRs) and a sandwiched TiO<sub>2</sub> thin layer was proposed to further enhance the nonlinear harmonic efficiency, as shown in Figure 3a.<sup>74</sup> The dispersion of the second harmonic roughly follows that of the transverse electric (TE) guided modes, indicating that the nonlinear enhancements mainly stem from the coherent collective scattering of the nonlocal guided modes. Due to the efficient spectral overlap between the fundamental LSPRs and the guided mode resonances, the suppressed radiative loss, and the effective excitation of the nonlinear polarizability in SRRs, the evaluated nonlinear enhancement factors enlarge by 2 orders of magnitude compared with the bare gold resonator metasurfaces. Additionally, metasurface-assisted on-chip nonlinear generations are free of phase matching thanks to the multiple in-plane momentum provided by different subwavelength nanoscatterers.<sup>88</sup> The efficient mode overlapping inside the waveguides and coherent superposition of nonlinear polarizability empower efficient nonlinear generation of the hybrid nanostructure, which is very promising for applications of photonic chips.

In addition to metasurfaces, trapped light in waveguides or nanocavities may probably be out-coupled and further manipulated by meticulous designs.<sup>22,89,90</sup> Figure 3b shows an example of circularly arranged, zigzagged aluminum nanorods on a silicon nitride microcavity with a coupled waveguide, which guides incident light with different spins to specific ports of the waveguide.<sup>75</sup> The relative coupling efficiency shown in

Figure 3b suggests that the waveguide mode with the opposite direction is excited when the incidence polarization changes from right-handed circularly polarized to left-handed circularly polarized, realizing the on-chip photonic spin Hall effect.<sup>75</sup> Similarly, considering the momentum-matching conditions between the local resonances and the nonlocal modes, a spin-selective directional coupler and wavelength demultiplexing device was proposed and demonstrated in waveguides integrated with metasurfaces.<sup>91</sup> In addition, the optical properties of the hybrid nanostructures involving nonlocal modes can be easily tailored by tuning different geometric parameters, providing a new route to couple and manipulate light fields bounded in microcavities and waveguides.

Another important class of artificial structures to achieve localization of electromagnetic fields is the Moiré lattice.<sup>92–94</sup> Figure 3c demonstrates the transition of local and nonlocal mode in an optical Moiré lattice made of photo-refractive crystals directly written by lasers.<sup>45</sup> Figure 3c clearly shows a phase diagram of (de)localizations in the parameter space, in which  $\theta$  describes the magic angle of the Moiré lattice and the potential depths of the sublattices are  $p_1$  and  $p_2$ , respectively. The mode localization and expansion can be tailored by the system parameters, namely, the magic angle and the two potential depths corresponding to the two sublattices, as shown in Figure 3c.<sup>45</sup> Recently, flat bands utilizing the interlayer couplings and/or intralayer couplings were demonstrated in twisted bilayer photonic slabs<sup>95</sup> and applied to angular-robust harmonic enhancements.<sup>96</sup> Enhanced second-harmonic generation with focused beam incidence was achieved thanks to the flat-band Moiré quasi-BICs.<sup>96</sup> The transition between local and nonlocal modes is expected to underpin flexible manipulation of optical harmonics, which is highly desirable in nonlinear optical switching and on-chip communications.

On the other hand, band engineering is a successful route to design local or nonlocal modes with distinct advantages.<sup>97,98</sup> Figure 3d shows a flat-envelope nonlocal mode supported by open photonic crystal cavities with a Dirac dispersion, which is counterintuitive.<sup>46</sup> In contrast to the common idea that one needs reflectors to build resonators, Contractor et al. proposed building a laser cavity with open boundary conditions.<sup>46</sup> The intriguing cavity maintains Dirac dispersion even with a finite dimension (scalable), which ensures the orthogonality of the symmetry-protected mode with the other two  $C_2$  symmetric modes near the Dirac point, as shown in Figure 3d. The symmetry-protected mode experiences zero effective refractive index and thus expands the whole nanostructure without phase retardation, as depicted in Figure 3d. The open Dirac cavities are made of InGaAsP multiple quantum wells to further generate single mode lasing by exploiting the flat-envelope nonlocal mode. Conventional finite-size microcavities have total-reflection or open boundaries without Dirac dispersions, and the modes are generally accompanied by Gaussian or high-order envelopes that satisfy the conditions for a standing wave.<sup>99</sup> In contrast, the open Dirac cavity supports a flat-envelope nonlocal mode that can avoid spatial hole burning effects, and the Dirac dispersion also enlarges the complex free spectral ranges between the lasing mode and the other undesirable high-order modes, which is very fascinating for high-power single-mode surface-emitting lasers.<sup>47,100,101</sup>

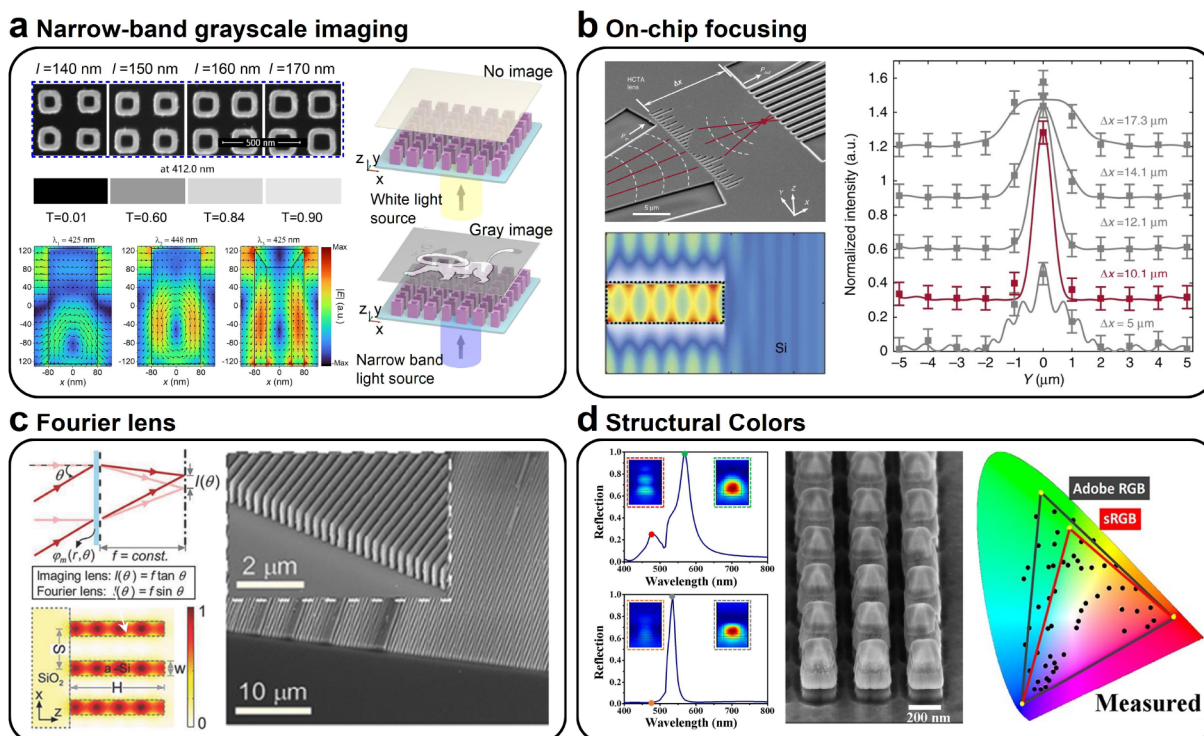


**Figure 4.** Applications of local and nonlocal metasurfaces. (a) SEM images of hollow Mie resonators with different transmittances corresponding to different scales. Mode profiles of the hollow Mie resonators. Illustration of narrow-band grayscale imaging using collective Mie resonances.<sup>102</sup> (b) SEM images of on-chip focusing using air-slot resonators as phase retarders. Mode distributions of the air-slot resonators in silicon waveguides. Received intensities by waveguide arrays showing a focusing behavior.<sup>103</sup> (c) Concept of the Fourier lens and the employed waveguide modes. SEM micrograph of the fabricated Fourier metalens composed of dielectric nanolines.<sup>104</sup> (d) Simulated reflection spectra of multilayer nanoblocks with suppressed Mie scattering at shorter wavelengths (lower panel), showing better monochromaticity than that of single-layer nanoblocks (upper panel). Measured colors in the CIE 1931 chromaticity coordinates, exceeding the Adobe RGB space.<sup>105</sup> (a) Reprinted with permission from ref 102. Copyright 2022 WILEY-VCH. (b) Reprinted under the terms of Creative Commons license (<https://creativecommons.org/licenses/by/4.0/>) from ref 103. Copyright 2019 the Authors, published by Nature Publishing Group. (c) Reprinted with permission from ref 106. Copyright 2018 WILEY-VCH. (d) Reprinted with permission from ref 105. Copyright 2019 American Chemical Society.

## APPLICATIONS

The aforementioned novel physical mechanisms involving both local and nonlocal modes have promoted many representative applications, which will be briefly summarized in this section. Based on high-*Q* collective Mie resonances supported by hollow rectangular nanopillar metasurfaces, the transmission amplitude can be tuned by the geometry of the hollow nanopillars, realizing narrow-band grayscale near-field imaging.<sup>102</sup> The fabricated samples and corresponding transmission intensities are shown in Figure 4a. The hollow rectangular nanopillars have higher *Q* factors than the original rectangular nanoblocks, and the corresponding electric field distributions show a confinement of Mie resonances, as illustrated in Figure 4a. Based on the narrow-band engineering of the amplitudes of light, frequency-selective optical encryption was further demonstrated.<sup>102</sup> In addition to the amplitudes of light, the phases and polarization states are expected to be manipulated by nanostructures involving high-*Q* nonlocal modes as well, achieving multiple intriguing functions such as optical coding and encryption, imaging, and spin detection.<sup>107–112</sup>

One important trend is on-chip light manipulation by metamaterials, which underpins the advances of photonic integrated circuits.<sup>89,90</sup> Recently, a hollow air slot array has been employed to offer phase modulations on in-plane propagating waveguide modes.<sup>103</sup> The schematic and SEM image are shown in Figure 4b. Focusing phases were applied to

the lights in the waveguides when traveling through an array of air slots. Then the focused light signals were collected by several tiny waveguide ports to monitor the focusing properties. The employed air slots with different lengths have different phase retardations, which stem from the propagation phase of the guided modes shown in Figure 4b. The focusing characteristics are depicted in Figure 4b, showing a good focusing performance at the focal plane. The ultracompact metasurface-integrated waveguides served as an on-chip metalens with an NA up to 2.14 and could focus light to within 10  $\mu\text{m}$  with less than 1 dB loss.<sup>103</sup> In addition, the authors demonstrated on-chip spatial Fourier transform and spatial differentiation in experiments as well, showing promising potentials in various applications such as ultracompact mode division multiplexing and on-chip optical computation.<sup>103</sup>

Another substantial application of artificial nanostructures is metalenses, which are expected to replace conventional bulk lenses due to their compact size and abilities to correct various aberrations.<sup>40,104,113</sup> With a tailored hyperbolic phase distribution, a metalens can convert a plane wavefront to a spherical wavefront with an ultracompact size, and various well-performing metalenses against one or more optical aberrations have been proposed in recent years.<sup>114–116</sup> However, most metalenses work under paraxial conditions because controlling the angular dispersions of the phase distribution is very challenging. Recently, Liu et al. proposed a wide-angle Fourier

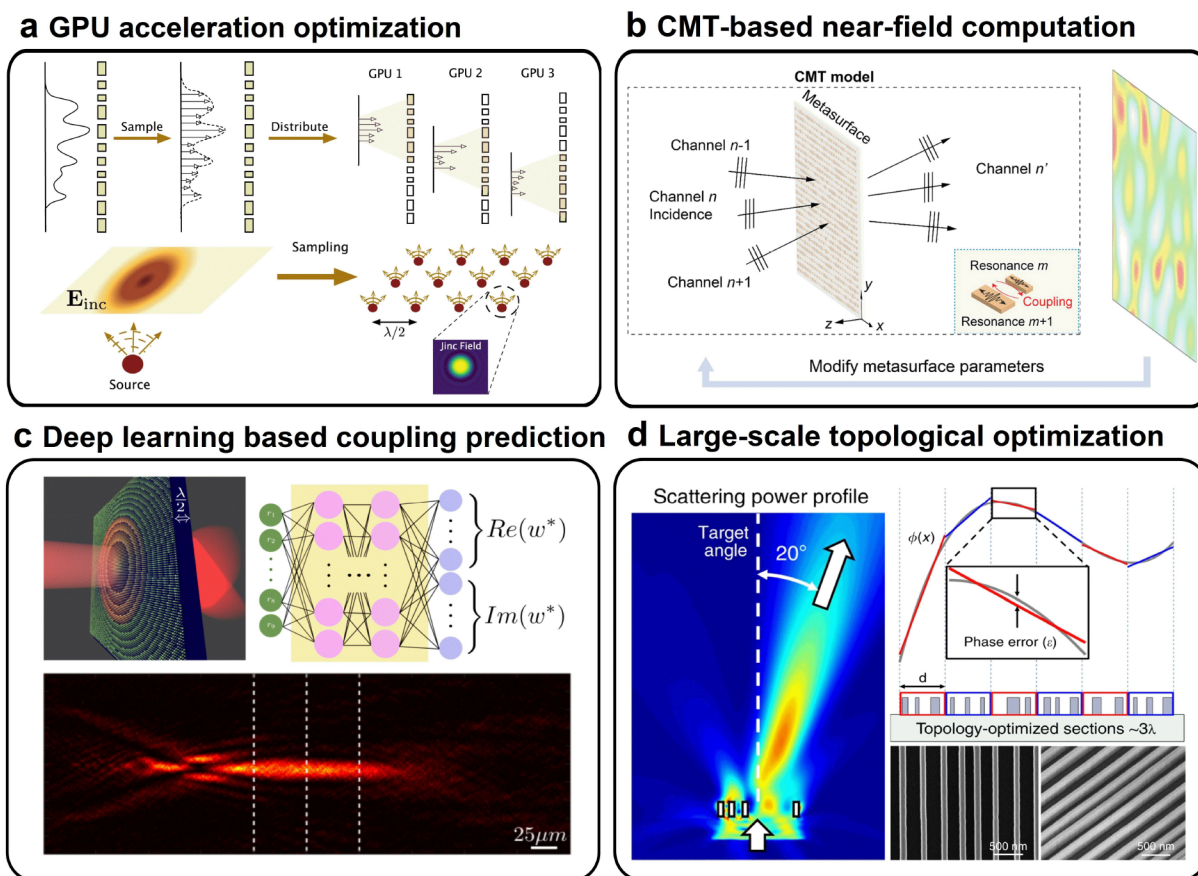


**Figure 5.** Examples of nonlocal metasurface optimized by different algorithms. (a) Computation of large-scale metasurfaces based on a T-matrix method with GPU acceleration.<sup>33</sup> (b) Coupled-mode-theory (CMT) computations on the far-field distributions of the metasurfaces with adjoint optimization.<sup>126</sup> (c) A metasurface design based on a deep neural network (DNN) to consider the coupling of adjacent resonators.<sup>127</sup> (d) Topologically optimized metasurfaces with a unit section of approximately  $3\lambda$ , in which the coupling between nanowaveguides is considered.<sup>128</sup> (a) Reprinted under the terms of Creative Commons license (<https://creativecommons.org/licenses/by/4.0/>) from ref 33. Copyright 2022 the Authors, published by Nature Publishing Group. (b) Reprinted with permission from ref 126. Copyright 2021 American Chemical Society. (c) Reprinted with permission from ref 127. Copyright 2021 American Chemical Society. (d) Reprinted under the terms of Creative Commons license (<https://creativecommons.org/licenses/by/4.0/>) from ref 128. Copyright 2019 the Authors, published by Nature Publishing Group.

lens up to  $60^\circ$  with 85% efficiency, as shown in Figure 4c.<sup>106</sup> Fourier lenses are perfect lenses for Fourier transforms due to the strict angular dispersion relations of the foci offset. Similar to the gradient metasurfaces, the phase distributions of the Fourier metalens were realized by tailoring the width of the consisting nanolines, as shown in Figure 4c. The large-angle dispersion of resonant phases is a haunting problem for dielectric Mie resonators, which was recently solved by employing waveguide modes inside the nanolines, as illustrated in Figure 4c. Due to the horizontal localization property of the vertically guided modes, flat-band effects maintain the phase functions of the metalens even in a large-angle incidence. The Fourier transform of a grating and the spatial filtering performed by the wide-angle Fourier lens were experimentally demonstrated as well.<sup>106</sup>

In addition to applications based on manipulations of the intensity, phases, and polarization states of light, implements achieved by engineering the spectrum of artificial nanostructures will be subsequently discussed. One significant application of optical artificial nanostructures is structural colors because of their distinct advantages in resolution, color purity, and stability.<sup>117,118</sup> Historically proposed in photonic crystals that can reflect photons with energy and momentum residing in the band gaps, structural colors are flourishing in

the research field of metasurfaces.<sup>119–121</sup> Based on the rich local and nonlocal modes, the spectrum in the visible band can be flexibly engineered.<sup>122–124</sup> However, the structural colors generated by simple plasmonic and dielectric nanostructures are generally limited by the relatively low color saturations. Recently, ultrahigh-saturation structural colors were theoretically proposed and experimentally demonstrated based on multilayer  $\text{TiO}_2$  metasurfaces.<sup>105</sup> The subtle multilayer design successfully suppresses the high-order Mie multipolar scattering of the single-layer metasurfaces by impedance matching on the nanostructure interfaces, as shown in Figure 4d. Consequently, the single Fano resonance peak dramatically enhances the monochromaticity of the reflection spectra, exhibiting more vivid colors. The theoretical and experimental color gamut can occupy 127% and 95% of the Adobe RGB space by tailoring the geometric parameters of the nanostructures. Colors with ultrahigh saturations are very promising for miniature high-end displays, advanced imaging, and vivid virtual reality technologies.<sup>125</sup>

## ■ ALGORITHM EMPOWERED NONLOCAL OPTIMIZATION

To exploit the near-field coupling between meta-atoms and expand the available degrees of freedom of the optical system,

various optimization algorithms have been applied to design metasurfaces. Conventionally, the target electromagnetic fields are constructed through a structural meta-atom library built from the full-wave simulation,<sup>107</sup> which is time-consuming to find the best solutions and the adjustable parameters are usually limited. Such a strategy requires negligible interactions between adjacent unit cells and is widely used in designs such as metalenses,<sup>115,129</sup> metaholography,<sup>130,131</sup> and multifunctional metasurfaces.<sup>132</sup> Moreover, the cost of time and computational resources grow exponentially with the expansion of the optimization area of the metasurface.<sup>133</sup> These difficulties impose many restrictions on structural designs, especially in the optimization of large-scale metasurfaces and the exploration of neighboring and nonlocal effects. Fortunately, with the upgrading of computing power and algorithms, some of the aforementioned problems can be effectively solved with the support of high-performance computers or well-designed algorithms. Recently, deep learning has attracted much attention because of its excellent abilities for feature extraction of physical effects and data fitting. Compared with conventional algorithms, deep learning has achieved outstanding performance in computer vision, automatic drive, and natural language processing. For metasurface research, deep learning also brings convenience for artificial nanostructure design and data analysis including forward prediction,<sup>41,134</sup> inverse design,<sup>135</sup> and result fittings.<sup>136,137</sup>

The most direct way to consider near fields with coupling effects is to compute the entire array. One of these numerical strategies to design and analyze large-scale metasurfaces is shown in Figure 5a.<sup>33</sup> The incident fields were first decomposed into a set of sources with distributions of *jinc* functions following the Nyquist sampling rule, and each source illuminates a part of the metasurface. Then, the divided metasurfaces and source arrays were parallelly distributed in several graphics processing units (GPUs) to compute the near-field interactions using the T-matrix method. Finally, a gradient-based method was applied to optimize the design parameters of the metasurface. The near-field calculation by the T-matrix method agrees well with the conventional full-wave simulations. Based on such a strategy, a metasurface consisting of silicon nanostructures with a size of  $645\lambda \times 645\lambda$  was calculated in 10 h, which is hard to address for traditional simulation software. The coupling between the nanostructures was also considered in the metasurface design by taking advantage of the large-scale computation. A metalens consisting of lower aspect ratio silicon scatterers was optimized, and the efficiency was improved from 0.1 (local field approximation) to 0.2 (nonlocal interactions) in 35 iterations.

In addition to direct calculations, the coupling effects can also be theoretically analyzed through the coupled-mode-theory (CMT). The coupled mode equations can be written as<sup>138</sup>

$$\frac{d}{dt}\mathbf{a} = \left( j\boldsymbol{\Omega} - \frac{\sum_{i=x,y,z} \mathbf{D}_i^\dagger \mathbf{D}_i}{2} \right) \mathbf{a} + \sum_{i=x,y,z} \mathbf{D}_i^T \mathbf{S}_{in}^{(i)}$$

$$\mathbf{S}_{out}^{(i)} = \mathbf{C}^{(i)} \mathbf{S}_{in}^{(i)} + \mathbf{D}_i \mathbf{a} \quad (1)$$

where  $\mathbf{a}$  is the complex amplitudes of the resonances and the matrices  $\mathbf{D}$ ,  $\mathbf{S}_{in}$  ( $\mathbf{S}_{out}$ ), and  $\mathbf{C}$  are the coupling coefficients, incoming (outgoing) waves, and background reflection and

transmission coefficients, respectively. The equation describes the relationship between the outgoing and incoming waves. Figure 5b shows a near-field optimization method based on the CMT, and the figure of merit (FOM) was calculated and optimized in the far-field.<sup>126</sup> Compared with traditional simulation methods, solving the CMT equations is advantageous to save computational resources, which enables large-area optimization of metasurfaces. Furthermore, an inverse-design-based adjoint optimization was applied to optimize the structure distribution of the metasurfaces, i.e., the design parameters were updated following the gradient of the FOM in every iteration step. A  $10000\lambda$  scale metalens with an NA of 0.9 can be obtained using CMT. Angle-multiplexed holograms were also presented in this work. Although the superiority of CMT-based optimization is remarkable, this strategy still has some restrictions, such as the requirement for the isolation of the resonance modes, limiting its applications in random shapes and materials.

Figure 5c shows another method to investigate the nonlocal interactions of nanostructures based on deep learning.<sup>127</sup> Taking the near-fields of nine random scatterers from the finite-difference time-domain (FDTD) simulation as the input data, a deep neural network that can extract the coupling features between the nanostructures was efficiently trained with TensorFlow. The neural network was trained and optimized with the near-field coupling incorporated by maximizing the FOM, which is defined as the difference between the calculated results and design target. An extended depth of focus (EDOF) lens with a focus depth of 100–350  $\mu\text{m}$  was achieved. The predicted results from the neural network are in good agreement with the FDTD simulations but require less solution time. Topological optimization is also popular in metasurface design because it can construct nanostructures with arbitrary shapes and designs. As shown in Figure 5d, topological optimization combined with adjoint simulation was employed to enhance the operating efficiency of the metalens.<sup>128</sup> Topological optimization usually treats the structure domain as an entirety to find the optimized material distributions, leading to dramatically increased computational requirements related to the device size. To overcome this disadvantage, the metasurface was divided into several sections at a  $3\lambda$ -scale, and topological optimization was performed in each section. In the forward adjoint simulation of each section, an aperiodic Fourier model method (AFMM) was employed to keep every section isolated. The optimization begins with a random dielectric distribution whose indices are between the air and the exact material and then updates the distribution with the iteration under the guidance of the gradient of FOM. After that, the material distribution is binarized to ensure feasibility in fabrication. Such a strategy can combine the advantages of topological optimization and unit design, with the size of the unit reaching several wavelengths. This work realized a metalens with a radius of 30  $\mu\text{m}$  and an NA of 0.2 to 0.9, and the improved working efficiency was verified through simulations and experiments.

## ■ SUMMARY AND OUTLOOK

In this Perspective, we have encapsulated various optical effects in the emerging field of artificial nanostructures involving local and nonlocal modes, including local and nonlocal resonance couplings, BICs, on-chip light manipulations and calculations, and control of mode (de)localizations. We reviewed the applications for optical field manipulations such as near-field

imaging, nonlinear harmonics generation, on-chip lens and Fourier operations, wide-angle Fourier lenses, and artificial structural colors. For a long time, many of those developments were established on direct assemblies of plasmonic nanoantennas and/or Mie resonators using local optical properties. However, metallic nanostructures suffer from severe ohmic loss in the visible and infrared bands, which hinders the development of highly efficient optical devices. On the other hand, Mie resonances supported by high-index dielectric nanostructures have inevitable neighboring interactions especially in nonlinear metasurfaces, causing difficulties in precisely harnessing the phase and amplitude distributions of the overall metasurfaces. Based on the comprehensive consideration of both the local resonances with abilities to confine electromagnetic fields on a subwavelength scale and the nonlocal collective modes involving the neighboring interactions, we envision efficient multifunctional nanostructures with high  $Q$  factors and strong frequency selectivity. The exclusive narrow-band and extended modal overlap properties are highly promising for applications such as augmented reality, controllable lasers, and nonlinear harmonic generations. We expect that rapid developments exploiting local and nonlocal modes will boost a range of significant innovations in integrated photonics and compact quantum chips and will provide foundations for next-generation of highly efficient multifunctional optical devices.

We next summarize the advantages and disadvantages of local and nonlocal resonances. The local modes can locally manipulate the optical fields, including optical amplitudes, phases, and polarization states, by the spatial arrangement of the nanoresonators, which are flexible and easy to develop. Local metasurfaces generally show broadband and wide-angle functionalities because of their lower  $Q$  factors and flat-band features. However, the lower  $Q$  factors of local modes limit their effective light–matter interaction distances for special functionalities and applications. On the other hand, nonlocal modes can support ultrahigh- $Q$  resonances such as BICs, which can dramatically enhance the efficiency of light–matter interactions<sup>70</sup> and are promising for narrow-band applications such as biosensing and multiplexing.<sup>139</sup> Nonlocal modes are dispersive and can be easily engineered in momentum space, which opens new degrees of freedom to manipulate optical fields. Furthermore, nonlocal modes are more robust to fabrication errors since their properties depend on the global effects of the nanostructures.<sup>62</sup>

Nonlocal modes are promising for metasurface applications, but there are still some challenges in the design of desiring optical fields by exploiting local and nonlocal modes. The first is the lack of theoretical underpinnings. To date, dealing with both local and nonlocal optical properties of nanostructures lacks effective and succinct theories and relies on large-scale simulations and optimizations because band theory and PB-phase are insufficient to describe hybrid local and nonlocal modes. Second, it is difficult to simultaneously achieve local modulations of optical responses and high  $Q$  factors. The introduced phase or amplitude modulations will inevitably lead to red/blue-shifts of the local resonances owing to the different neighboring coupling conditions, so that the spectral overlap among meta-atoms becomes very low when the  $Q$  factors are extremely high, resulting in low efficiency of the overall functional metasurfaces. Another challenge is the absence of desirable materials with a high refractive index in the optical band to control couplings between local and nonlocal

resonances by tailoring the refractive index contrast, which is much easier in the microwave band.

In this Perspective, we provide several future directions for local and nonlocal nanostructures. Importantly, resonant nanostructures are attractive for enhancing and tailoring nonlinear harmonic signals because of their ability to trap light at the nanoscale. However, the temporal trapping of electromagnetic fields is not satisfying because of the intrinsic loss of plasmonic structures. On the other hand, dielectric nonlinear metasurfaces generally employ low- $Q$  Mie modes to manipulate nonlinear phases, amplitudes, or polarization states,<sup>140–143</sup> and the functionalities of ultrahigh- $Q$  nonlinear metasurfaces are limited because it is difficult to modulate nonlinear phases and amplitudes without sacrificing  $Q$  factors. It is known that high  $Q$  factors are critical for nonlinear enhancements and highly efficient nonlinear devices. Therefore, functional nonlinear metasurfaces with ultrahigh  $Q$  factors and nonlinear conversion efficiencies are in high demand.

The interplay between local and nonlocal modes employing novel materials such as semiconductors, nonlinear Kerr materials, and 2D materials is another frontier area in the field of light manipulation. The excited polaritons in the metasurfaces made of semiconductor materials can be easily controlled by the gate voltage and one can accordingly manipulate the corresponding mode couplings. It is believed that many nontrivial phenomena concerning interactions between various polaritons and nonlocal modes will be revealed in the near future.<sup>144,145</sup> For example, exploiting the topological band behaviors of hexagonal boron nitride (hBN) metagrating, the deep-subwavelength canalization of polaritons was achieved and observed based on strong near-field polaritonic couplings.<sup>146</sup> Hybrid nonlocal metasurfaces supported by low-loss dielectric resonators and emerging semiconductor nanostructures are expected to provide new opportunities for highly efficient and versatile photonic devices, with the underpinning physics being gradually elucidated in recent years.<sup>147</sup>

Owing to the extended nature of nonlocal modes, functional nanostructure arrays are challenging to design because the resonance modes are sensitive to both the geometric setup and lattice arrangement of resonators. As a result, a feedback-based simulation or optimization is required to fulfill the function of the device,<sup>21</sup> leading to time-consuming optimization, especially in a high-dimensional parameter space. For example, the deep-learning-based method usually requires tremendous training data that are obtained by full-wave simulations. Therefore, the cost of computation will grow exponentially with increasing degrees of freedom to obtain global functions involving nonlocal effects. To overcome the difficulty in optimization, several newly developed deep learning models, such as Transformer<sup>148</sup> and graph neural network (GNN),<sup>149</sup> may potentially find their applications in metasurface designs owing to their excellent capacities in extracting features and predicting results with higher accuracy than simple neural networks such as multilayer perceptron (MLP). Another challenge is that the design target (figure of merit) may converge to a local extremum point or a saddle point but not the global optimum, especially for metasurfaces with a high-dimensional parameter space and significant nonlocal effects. Fast convergence and global optimization can be obtained by combining the physical model and a neural network to predict the nonlocal effects based on a smaller data set and improve the prediction accuracy. The solution to these design

difficulties may provide many more possibilities for nanophotonics with integrated multiple metasystems.

## AUTHOR INFORMATION

### Corresponding Authors

**Wenwei Liu** – The Key Laboratory of Weak Light Nonlinear Photonics, Ministry of Education, School of Physics and TEDA Institute of Applied Physics, Renewable Energy Conversion and Storage Center, Smart Sensing Interdisciplinary Science Center, Nankai University, 300071 Tianjin, China; Email: [wliu@nankai.edu.cn](mailto:wliu@nankai.edu.cn)

**Hua Cheng** – The Key Laboratory of Weak Light Nonlinear Photonics, Ministry of Education, School of Physics and TEDA Institute of Applied Physics, Renewable Energy Conversion and Storage Center, Smart Sensing Interdisciplinary Science Center, Nankai University, 300071 Tianjin, China; Email: [hcheng@nankai.edu.cn](mailto:hcheng@nankai.edu.cn)

**Shuqi Chen** – The Key Laboratory of Weak Light Nonlinear Photonics, Ministry of Education, School of Physics and TEDA Institute of Applied Physics, Renewable Energy Conversion and Storage Center, Smart Sensing Interdisciplinary Science Center, Nankai University, 300071 Tianjin, China; The Collaborative Innovation Center of Extreme Optics, Shanxi University, Taiyuan 030006 Shanxi, China; Collaborative Innovation Center of Light Manipulations and Applications, Shandong Normal University, 250358 Jinan, China; [orcid.org/0000-0002-7898-4148](https://orcid.org/0000-0002-7898-4148); Email: [schen@nankai.edu.cn](mailto:schen@nankai.edu.cn)

### Authors

**Ruoheng Chai** – The Key Laboratory of Weak Light Nonlinear Photonics, Ministry of Education, School of Physics and TEDA Institute of Applied Physics, Renewable Energy Conversion and Storage Center, Smart Sensing Interdisciplinary Science Center, Nankai University, 300071 Tianjin, China

**Qi Liu** – The Key Laboratory of Weak Light Nonlinear Photonics, Ministry of Education, School of Physics and TEDA Institute of Applied Physics, Renewable Energy Conversion and Storage Center, Smart Sensing Interdisciplinary Science Center, Nankai University, 300071 Tianjin, China

**Zhancheng Li** – The Key Laboratory of Weak Light Nonlinear Photonics, Ministry of Education, School of Physics and TEDA Institute of Applied Physics, Renewable Energy Conversion and Storage Center, Smart Sensing Interdisciplinary Science Center, Nankai University, 300071 Tianjin, China

**Jianguo Tian** – The Key Laboratory of Weak Light Nonlinear Photonics, Ministry of Education, School of Physics and TEDA Institute of Applied Physics, Renewable Energy Conversion and Storage Center, Smart Sensing Interdisciplinary Science Center, Nankai University, 300071 Tianjin, China

Complete contact information is available at:

<https://pubs.acs.org/10.1021/acsp Photonics.2c01534>

### Notes

The authors declare no competing financial interest.

## ACKNOWLEDGMENTS

This work was supported by the National Key Research and Development Program of China (2021YFA1400601 and

2022YFA1404501), the National Natural Science Fund for Distinguished Young Scholars (11925403), and the National Natural Science Foundation of China (12122406, 12192253, 11974193, 12274237, 12274239, and U22A20258).

## REFERENCES

- (1) Yao, K.; Liu, Y. Plasmonic metamaterials. *Nanotechnol. Rev.* **2014**, *3*, 177–210.
- (2) Joannopoulos, J. D.; Johnson, S. G.; Winn, J. N.; Meade, R. D. *Photonic Crystals: Molding the Flow of Light*, 2nd ed.; Princeton University Press: Princeton, NJ, United States, 2011.
- (3) Jahani, S.; Jacob, Z. All-dielectric metamaterials. *Nat. Nanotechnol.* **2016**, *11*, 23–26.
- (4) Kivshar, Y.; Miroshnichenko, A. Meta-optics with Mie resonances. *Opt. Photonics News* **2017**, *28*, 24–31.
- (5) Kruk, S.; Kivshar, Y. Functional meta-optics and nanophotonics govern by Mie resonances. *ACS Photonics* **2017**, *4*, 2638–2649.
- (6) Koshelev, K.; Kivshar, Y. Dielectric resonant metaphotonics. *ACS Photonics* **2021**, *8*, 102–112.
- (7) Qin, J.; Jiang, S.; Wang, Z.; Cheng, X.; Li, B.; Shi, Y.; Tsai, D.-P.; Liu, A.-Q.; Huang, W.; Zhu, W. Metasurface micro/nano-optical sensors: principles and applications. *ACS Nano* **2022**, *16*, 11598–11618.
- (8) Dixon, J.; Lawrence, M.; Barton, D. R.; Dionne, J. Self-isolated raman lasing with a chiral dielectric metasurface. *Phys. Rev. Lett.* **2021**, *126*, 123201.
- (9) Sarychev, A. K.; Ivanov, A.; Lagarkov, A. N.; Ryzhikov, I.; Afanasev, K.; Bykov, I.; Barbillon, G.; Bakholdin, N.; Mikhailov, M.; Smyk, A.; Shurygin, A.; Shalygin, A. Plasmon localization and giant fields in an open-resonator metasurface for surface-enhanced-Raman-scattering sensors. *Phys. Rev. Appl.* **2022**, *17*, 044029.
- (10) Yu, Y.; Sakanas, A.; Zali, A. R.; Semenova, E.; Yvind, K.; Mørk, J. Ultra-coherent Fano laser based on a bound state in the continuum. *Nat. Photonics* **2021**, *15*, 758–764.
- (11) Koshelev, K.; Kruk, S.; Melik-Gaykazyan, E.; Choi, J.-H.; Bogdanov, A.; Park, H.-G.; Kivshar, Y. Subwavelength dielectric resonators for nonlinear nanophotonics. *Science* **2020**, *367*, 288–292.
- (12) Chen, S.; Liu, W.; Li, Z.; Cheng, H.; Tian, J. Metasurface-empowered optical multiplexing and multifunction. *Adv. Mater.* **2020**, *32*, 1805912.
- (13) Sakoda, K. *Optical Properties of Photonic Crystals*; Springer: Berlin, 2005; Vol. 2.
- (14) Zhu, W.; Zheng, H.; Zhong, Y.; Yu, J.; Chen, Z. Wave-vector-varying Pancharatnam-Berry phase photonic spin Hall effect. *Phys. Rev. Lett.* **2021**, *126*, 083901.
- (15) Yu, N.; Genevet, P.; Kats, M. A.; Aieta, F.; Tetienne, J.-P.; Capasso, F.; Gaburro, Z. Light propagation with phase discontinuities: generalized laws of reflection and refraction. *Science* **2011**, *334*, 333–337.
- (16) Song, Q.; Odeh, M.; Zúñiga-Pérez, J.; Kanté, B.; Genevet, P. Plasmonic topological metasurface by encircling an exceptional point. *Science* **2021**, *373*, 1133–1137.
- (17) Vahala, K. J. Optical microcavities. *Nature* **2003**, *424*, 839–846.
- (18) Utyushev, A. D.; Zakomirnyi, V. I.; Rasskazov, I. L. Collective lattice resonances: Plasmonics and beyond. *Rev. Phys.* **2021**, *6*, 100051.
- (19) Zakomirnyi, V.; Ershov, A.; Gerasimov, V.; Karpov, S.; Ågren, H.; Rasskazov, I. Collective lattice resonances in arrays of dielectric nanoparticles: a matter of size. *Opt. Lett.* **2019**, *44*, 5743–5746.
- (20) Bogdanov, A. A.; Koshelev, K. L.; Kapitanova, P. V.; Rybin, M. V.; Gladyshev, S. A.; Sadrieva, Z. F.; Samusev, K. B.; Kivshar, Y. S.; Limonov, M. F. Bound states in the continuum and Fano resonances in the strong mode coupling regime. *Adv. Photonics* **2019**, *1*, 016001.
- (21) Overvig, A. C.; Malek, S. C.; Yu, N. Multifunctional nonlocal metasurfaces. *Phys. Rev. Lett.* **2020**, *125*, 017402.
- (22) Huang, H.; Overvig, A. C.; Xu, Y.; Malek, S. C.; Tsai, C.-C.; Alù, A.; Yu, N. Leaky-wave metasurfaces for integrated photonics.

arXiv:2207.08936 (physics.optics) 2022-07-18, <https://arxiv.org/abs/2207.08936>. (accessed 2022-12-08).

(23) Malek, S. C.; Overvig, A. C.; Alù, A.; Yu, N. Multifunctional resonant wavefront-shaping meta-optics based on multilayer and multi-perturbation nonlocal metasurfaces. *Light Sci. Appl.* **2022**, *11*, 246.

(24) Malek, S. C.; Overvig, A. C.; Shrestha, S.; Yu, N. Active nonlocal metasurfaces. *Phys. Rev. Lett.* **2020**, *10*, 655–665.

(25) Overvig, A.; Alù, A. Wavefront-selective Fano resonant metasurfaces. *Adv. Photonics* **2021**, *3*, 026002.

(26) Overvig, A.; Yu, N.; Alù, A. Chiral quasi-bound states in the continuum. *Phys. Rev. Lett.* **2021**, *126*, 073001.

(27) Marinica, D.; Borisov, A.; Shabanov, S. Bound states in the continuum in photonics. *Phys. Rev. Lett.* **2008**, *100*, 183902.

(28) Hsu, C. W.; Zhen, B.; Stone, A. D.; Joannopoulos, J. D.; Soljačić, M. Bound states in the continuum. *Nat. Rev. Mater.* **2016**, *1*, 16048.

(29) Lee, J.; Zhen, B.; Chua, S.-L.; Qiu, W.; Joannopoulos, J. D.; Soljačić, M.; Shapira, O. Observation and differentiation of unique high-Q optical resonances near zero wave vector in macroscopic photonic crystal slabs. *Phys. Rev. Lett.* **2012**, *109*, 067401.

(30) Overvig, A. C.; Mann, S. A.; Alù, A. Thermal metasurfaces: complete emission control by combining local and nonlocal light-matter interactions. *Phys. Rev. X* **2021**, *11*, 021050.

(31) Koshelev, K.; Lepeshov, S.; Liu, M.; Bogdanov, A.; Kivshar, Y. Asymmetric metasurfaces with high-Q resonances governed by bound states in the continuum. *Phys. Rev. Lett.* **2018**, *121*, 193903.

(32) Overvig, A.; Alù, A. Diffractive nonlocal metasurfaces. *Laser Photonics Rev.* **2022**, *16*, 2100633.

(33) Skarda, J.; Trivedi, R.; Su, L.; Ahmad-Stein, D.; Kwon, H.; Han, S.; Fan, S.; Vučković, J. Low-overhead distribution strategy for simulation and optimization of large-area metasurfaces. *Npj Comput. Mater.* **2022**, *8*, 78.

(34) Gao, X.; Yang, L.; Lin, H.; Zhang, L.; Li, J.; Bo, F.; Wang, Z.; Lu, L. Dirac-vortex topological cavities. *Nat. Nanotechnol.* **2020**, *15*, 1012–1018.

(35) Yu, N.; Capasso, F. Flat optics with designer metasurfaces. *Nat. Mater.* **2014**, *13*, 139–150.

(36) Liu, W.; Li, Z.; Cheng, H.; Chen, S.; Tian, J. Momentum analysis for metasurfaces. *Phys. Rev. Appl.* **2017**, *8*, 014012.

(37) Yu, S.; Li, Z.; Liu, W.; Cheng, H.; Zhang, Y.; Xie, B.; Zhou, W.; Tian, J.; Chen, S. Tunable dual-band and high-quality-factor perfect absorption based on VO<sub>2</sub>-assisted metasurfaces. *Opt. Express* **2021**, *29*, 31488–31498.

(38) Li, Z.; Liu, W.; Ma, D.; Yu, S.; Cheng, H.; Choi, D.-Y.; Tian, J.; Chen, S. Inverse design of few-layer metasurfaces empowered by the matrix theory of multilayer optics. *Phys. Rev. Appl.* **2022**, *17*, 024008.

(39) Li, G.; Zhang, S.; Zentgraf, T. Nonlinear photonic metasurfaces. *Nat. Rev. Mater.* **2017**, *2*, 17010.

(40) Pan, M.; Fu, Y.; Zheng, M.; Chen, H.; Zang, Y.; Duan, H.; Li, Q.; Qiu, M.; Hu, Y. Dielectric metalens for miniaturized imaging systems: progress and challenges. *Light Sci. Appl.* **2022**, *11*, 195.

(41) Ma, D.; Li, Z.; Liu, W.; Geng, G.; Cheng, H.; Li, J.; Tian, J.; Chen, S. Deep-learning enabled multicolor meta-holography. *Adv. Opt. Mater.* **2022**, *10*, 2102628.

(42) Li, Z.; Liu, W.; Geng, G.; Li, Z.; Li, J.; Cheng, H.; Chen, S.; Tian, J. Multiplexed nondiffracting nonlinear metasurfaces. *Adv. Funct. Mater.* **2020**, *30*, 1910744.

(43) Xie, Y.-Y.; Ni, P.-N.; Wang, Q.-H.; Kan, Q.; Briere, G.; Chen, P.-P.; Zhao, Z.-Z.; Delga, A.; Ren, H.-R.; Chen, H.-D.; Xu, C.; Genevet, P. Metasurface-integrated vertical cavity surface-emitting lasers for programmable directional lasing emissions. *Nat. Nanotechnol.* **2020**, *15*, 125–130.

(44) Song, J.-H.; van de Groep, J.; Kim, S. J.; Brongersma, M. L. Non-local metasurfaces for spectrally decoupled wavefront manipulation and eye tracking. *Nat. Nanotechnol.* **2021**, *16*, 1224–1230.

(45) Wang, P.; Zheng, Y.; Chen, X.; Huang, C.; Kartashov, Y. V.; Torner, L.; Konotop, V. V.; Ye, F. Localization and delocalization of light in photonic moiré lattices. *Nature* **2020**, *577*, 42–46.

(46) Contractor, R.; Noh, W.; Redjem, W.; Qarony, W.; Martin, E.; Dhuey, S.; Schwartzberg, A.; Kanté, B. Scalable single-mode surface-emitting laser via open-Dirac singularities. *Nature* **2022**, *608*, 692–698.

(47) Yang, L.; Li, G.; Gao, X.; Lu, L. Topological-cavity surface-emitting laser. *Nat. Photonics* **2022**, *16*, 279–283.

(48) Rybin, M. V.; Filonov, D. S.; Samusev, K. B.; Belov, P. A.; Kivshar, Y. S.; Limonov, M. F. Phase diagram for the transition from photonic crystals to dielectric metamaterials. *Nat. Commun.* **2015**, *6*, 10102.

(49) Yu, S.; Qiu, C.-W.; Chong, Y.; Torquato, S.; Park, N. Engineered disorder in photonics. *Nat. Rev. Mater.* **2021**, *6*, 226–243.

(50) Sun, S.; Yang, K.-Y.; Wang, C.-M.; Juan, T.-K.; Chen, W. T.; Liao, C. Y.; He, Q.; Xiao, S.; Kung, W.-T.; Guo, G.-Y.; et al. High-efficiency broadband anomalous reflection by gradient meta-surfaces. *Nano Lett.* **2012**, *12*, 6223–6229.

(51) Baur, S.; Sanders, S.; Manjavacas, A. Hybridization of lattice resonances. *ACS Nano* **2018**, *12*, 1618–1629.

(52) Quaranta, G.; Basset, G.; Martin, O. J.; Gallinet, B. Recent advances in resonant waveguide gratings. *Laser Photonics Rev.* **2018**, *12*, 1800017.

(53) Deng, Z.-L.; Li, F.-J.; Li, H.; Li, X.; Alù, A. Extreme diffraction control in metagratings leveraging bound states in the continuum and exceptional points. *Laser Photonics Rev.* **2022**, *16*, 2100617.

(54) Azzam, S. I.; Shalae, V. M.; Boltasseva, A.; Kildishev, A. V. Formation of bound states in the continuum in hybrid plasmonic-photonic systems. *Phys. Rev. Lett.* **2018**, *121*, 253901.

(55) Kikkawa, R.; Nishida, M.; Kadoya, Y. Polarization-based branch selection of bound states in the continuum in dielectric waveguide modes anti-crossed by a metal grating. *New J. Phys.* **2019**, *21*, 113020.

(56) Xiang, J.; Xu, Y.; Chen, J.-D.; Lan, S. Tailoring the spatial localization of bound state in the continuum in plasmonic-dielectric hybrid system. *Nanophotonics* **2020**, *9*, 133–142.

(57) Wang, W.; Wang, L.-Q.; Xue, R.-D.; Chen, H.-L.; Guo, R.-P.; Liu, Y.; Chen, J. Unidirectional excitation of radiative-loss-free surface plasmon polaritons in PT-symmetric systems. *Phys. Rev. Lett.* **2017**, *119*, 077401.

(58) Hsu, C. W.; Zhen, B.; Lee, J.; Chua, S.-L.; Johnson, S. G.; Joannopoulos, J. D.; Soljačić, M. Observation of trapped light within the radiation continuum. *Nature* **2013**, *499*, 188–191.

(59) Koshelev, K.; Bogdanov, A.; Kivshar, Y. Engineering with bound states in the continuum. *Opt. Photonics News* **2020**, *31*, 38–45.

(60) Zhen, B.; Hsu, C. W.; Lu, L.; Stone, A. D.; Soljačić, M. Topological nature of optical bound states in the continuum. *Phys. Rev. Lett.* **2014**, *113*, 257401.

(61) Zhang, Y.; Chen, A.; Liu, W.; Hsu, C. W.; Wang, B.; Guan, F.; Liu, X.; Shi, L.; Lu, L.; Zi, J. Observation of polarization vortices in momentum space. *Phys. Rev. Lett.* **2018**, *120*, 186103.

(62) Jin, J.; Yin, X.; Ni, L.; Soljačić, M.; Zhen, B.; Peng, C. Topologically enabled ultrahigh-Q guided resonances robust to out-of-plane scattering. *Nature* **2019**, *574*, 501–504.

(63) Kang, M.; Zhang, S.; Xiao, M.; Xu, H. Merging bound states in the continuum at off-high symmetry points. *Phys. Rev. Lett.* **2021**, *126*, 117402.

(64) Chai, R.; Liu, W.; Li, Z.; Cheng, H.; Tian, J.; Chen, S. Multiband quasibound states in the continuum engineered by space-group-invariant metasurfaces. *Phys. Rev. B* **2021**, *104*, 075149.

(65) Lee, S.-G.; Kim, S.-H.; Kee, C.-S. Metasurfaces with bound states in the continuum enabled by eliminating first Fourier harmonic component in lattice parameters. *Phys. Rev. Lett.* **2021**, *126*, 013601.

(66) Lee, S.-G.; Kim, S.-H.; Kee, C.-S. Bound states in the continuum (BIC) accompanied by avoided crossings in leaky-mode photonic lattices. *Nanophotonics* **2020**, *9*, 4373–4380.

(67) Lee, S.-G.; Kim, S.-H.; Kee, C.-S. Fourier-component engineering to control light diffraction beyond subwavelength limit. *Nanophotonics* **2021**, *10*, 3917–3925.

(68) Lee, S.-G.; Kim, S.-H.; Kee, C.-S. Band dynamics accompanied by bound states in the continuum at the third-order  $\Gamma$  point in leaky-mode photonic lattices. *Photonics Res.* **2021**, *9*, 1109–1116.

- (69) Kwon, H.; Sounas, D.; Cordaro, A.; Polman, A.; Alù, A. Nonlocal metasurfaces for optical signal processing. *Phys. Rev. Lett.* **2018**, *121*, 173004.
- (70) Liu, Z.; Xu, Y.; Lin, Y.; Xiang, J.; Feng, T.; Cao, Q.; Li, J.; Lan, S.; Liu, J. High-Q quasibound states in the continuum for nonlinear metasurfaces. *Phys. Rev. Lett.* **2019**, *123*, 253901.
- (71) Overvig, A. C.; Malek, S. C.; Carter, M. J.; Shrestha, S.; Yu, N. Selection rules for quasibound states in the continuum. *Phys. Rev. B* **2020**, *102*, 035434.
- (72) Klopfer, E.; Lawrence, M.; Barton, D. R., III; Dixon, J.; Dionne, J. A. Dynamic focusing with high-quality-factor metalenses. *Nano Lett.* **2020**, *20*, 5127–5132.
- (73) Lawrence, M.; Barton, D. R., III; Dixon, J.; Song, J.-H.; van de Groep, J.; Brongersma, M. L.; Dionne, J. A. High quality factor phase gradient metasurfaces. *Nat. Nanotechnol.* **2020**, *15*, 956–961.
- (74) Abir, T.; Tal, M.; Ellenbogen, T. Second-harmonic enhancement from a nonlinear plasmonic metasurface coupled to an optical waveguide. *Nano Lett.* **2022**, *22*, 2712–2717.
- (75) Zhang, Y.; Li, Z.; Liu, W.; Li, Z.; Cheng, H.; Tian, J.; Chen, S. Multi-band on-chip photonic spin Hall effect and selective excitation of whispering gallery modes with metasurface-integrated microcavity. *Opt. Lett.* **2021**, *46*, 3528–3531.
- (76) Ye, W.; Zeuner, F.; Li, X.; Reineke, B.; He, S.; Qiu, C.-W.; Liu, J.; Wang, Y.; Zhang, S.; Zentgraf, T. Spin and wavelength multiplexed nonlinear metasurface holography. *Nat. Commun.* **2016**, *7*, 11930.
- (77) Krasnok, A.; Tymchenko, M.; Alù, A. Nonlinear metasurfaces: a paradigm shift in nonlinear optics. *Mater. Today* **2018**, *21*, 8–21.
- (78) Koshelev, K.; Tang, Y.; Li, K.; Choi, D.-Y.; Li, G.; Kivshar, Y. Nonlinear metasurfaces governed by bound states in the continuum. *ACS Photonics* **2019**, *6*, 1639–1644.
- (79) Hao, Z.; Liu, W.; Li, Z.; Li, Z.; Geng, G.; Wang, Y.; Cheng, H.; Ahmed, H.; Chen, X.; Li, J.; Tian, J.; Chen, S. Full complex-amplitude modulation of second harmonic generation with nonlinear metasurfaces. *Laser Photonics Rev.* **2021**, *15*, 2100207.
- (80) Ye, F.; Yu, Y.; Xi, X.; Sun, X. Second-harmonic generation in etchless lithium niobate nanophotonic waveguides with bound states in the continuum. *Laser Photonics Rev.* **2022**, *16*, 2100429.
- (81) Ma, M.; Li, Z.; Liu, W.; Tang, C.; Li, Z.; Cheng, H.; Li, J.; Chen, S.; Tian, J. Optical Information multiplexing with nonlinear coding metasurfaces. *Laser Photonics Rev.* **2019**, *13*, 1900045.
- (82) Li, Z.; Liu, W.; Li, Z.; Tang, C.; Cheng, H.; Li, J.; Chen, X.; Chen, S.; Tian, J. Nonlinear metasurfaces: tripling the capacity of optical vortices by nonlinear metasurface. *Laser Photonics Rev.* **2018**, *12*, 1870049.
- (83) Gao, Y.; Fan, Y.; Wang, Y.; Yang, W.; Song, Q.; Xiao, S. Nonlinear holographic all-dielectric metasurfaces. *Nano Lett.* **2018**, *18*, 8054–8061.
- (84) Zograf, G.; Koshelev, K.; Zalagina, A.; Korolev, V.; Hollinger, R.; Choi, D.-Y.; Zuerch, M.; Spielmann, C.; Luther-Davies, B.; Kartashov, D.; Makarov, S. V.; Kruk, S. S.; Kivshar, Y. High-harmonic generation from resonant dielectric metasurfaces empowered by bound states in the continuum. *ACS Photonics* **2022**, *9*, 567–574.
- (85) Liu, Z.; Wang, J.; Chen, B.; Wei, Y.; Liu, W.; Liu, J. Giant enhancement of continuous wave second harmonic generation from few-layer GaSe coupled to high-Q quasi bound states in the continuum. *Nano Lett.* **2021**, *21*, 7405–7410.
- (86) Kruk, S. S.; Wang, L.; Sain, B.; Dong, Z.; Yang, J.; Zentgraf, T.; Kivshar, Y. Asymmetric parametric generation of images with nonlinear dielectric metasurfaces. *Nat. Photonics* **2022**, *16*, 561–565.
- (87) Li, Z.; Liu, W.; Li, Z.; Cheng, H.; Chen, S.; Tian, J. Fano-resonance-based mode-matching hybrid metasurface for enhanced second-harmonic generation. *Opt. Lett.* **2017**, *42*, 3117–3120.
- (88) Wang, C.; Li, Z.; Kim, M.-H.; Xiong, X.; Ren, X.-F.; Guo, G.-C.; Yu, N.; Lončar, M. Metasurface-assisted phase-matching-free second harmonic generation in lithium niobate waveguides. *Nat. Commun.* **2017**, *8*, 2098.
- (89) Li, Z.; Kim, M.-H.; Wang, C.; Han, Z.; Shrestha, S.; Overvig, A. C.; Lu, M.; Stein, A.; Agarwal, A. M.; Lončar, M.; Yu, N. Controlling propagation and coupling of waveguide modes using phase-gradient metasurfaces. *Nat. Nanotechnol.* **2017**, *12*, 675–683.
- (90) Meng, Y.; et al. Optical meta-waveguides for integrated photonics and beyond. *Light Sci. Appl.* **2021**, *10*, 235.
- (91) Zhang, Y.; Li, Z.; Liu, W.; Li, Z.; Cheng, H.; Chen, S.; Tian, J. Spin-selective and wavelength-selective demultiplexing based on waveguide-integrated all-dielectric metasurfaces. *Adv. Opt. Mater.* **2019**, *7*, 1801273.
- (92) Wu, Z.; Zheng, Y. Moiré metamaterials and metasurfaces. *Adv. Opt. Mater.* **2018**, *6*, 1701057.
- (93) Mao, X.-R.; Shao, Z.-K.; Luan, H.-Y.; Wang, S.-L.; Ma, R.-M. Magic-angle lasers in nanostructured moiré superlattice. *Nat. Nanotechnol.* **2021**, *16*, 1099–1105.
- (94) Mak, K. F.; Shan, J. Semiconductor moiré materials. *Nat. Nanotechnol.* **2022**, *17*, 686–695.
- (95) Nguyen, H. S.; Dubois, F.; Deschamps, T.; Cuffe, S.; Pardon, A.; Leclercq, J.-L.; Seassal, C.; Letartre, X.; Viktorovitch, P. Symmetry breaking in photonic crystals: on-demand dispersion from flatband to dirac cones. *Phys. Rev. Lett.* **2018**, *120*, 066102.
- (96) Huang, L.; Zhang, W.; Zhang, X. Moiré quasibound states in the continuum. *Phys. Rev. Lett.* **2022**, *128*, 253901.
- (97) Chua, S.-L.; Lu, L.; Bravo-Abad, J.; Joannopoulos, J. D.; Soljačić, M. Larger-area single-mode photonic crystal surface-emitting lasers enabled by an accidental Dirac point. *Opt. Lett.* **2014**, *39*, 2072–2075.
- (98) Zhen, B.; Hsu, C. W.; Igarashi, Y.; Lu, L.; Kaminer, I.; Pick, A.; Chua, S.-L.; Joannopoulos, J. D.; Soljačić, M. Spawning rings of exceptional points out of Dirac cones. *Nature* **2015**, *525*, 354–358.
- (99) Chen, Z.; Yin, X.; Jin, J.; Zheng, Z.; Zhang, Z.; Wang, F.; He, L.; Zhen, B.; Peng, C. Observation of miniaturized bound states in the continuum with ultra-high quality factors. *Sci. Bull.* **2022**, *67*, 359–366.
- (100) Eaton, S. W.; Fu, A.; Wong, A. B.; Ning, C.-Z.; Yang, P. Semiconductor nanowire lasers. *Nat. Rev. Mater.* **2016**, *1*, 16028.
- (101) Ma, R.-M.; Oulton, R. F. Applications of nanolasers. *Nat. Nanotechnol.* **2019**, *14*, 12–22.
- (102) Li, Z.; Geng, G.; Cheng, J.; Liu, W.; Yu, S.; Xie, B.; Cheng, H.; Li, J.; Zhou, W.; Tian, J.; Chen, S. Flexible confinement and manipulation of Mie resonances via nano rectangular hollow metasurfaces. *Adv. Opt. Mater.* **2022**, *10*, 2200185.
- (103) Wang, Z.; Li, T.; Soman, A.; Mao, D.; Kananen, T.; Gu, T. On-chip wavefront shaping with dielectric metasurface. *Nat. Commun.* **2019**, *10*, 3547.
- (104) Liu, W.; Cheng, H.; Tian, J.; Chen, S. Diffractive metalens: from fundamentals, practical applications to current trends. *Adv. Phys.: X* **2020**, *5*, 1742584.
- (105) Yang, B.; Liu, W.; Li, Z.; Cheng, H.; Choi, D.-Y.; Chen, S.; Tian, J. Ultra-highly saturated structural colors enhanced by multipolar-modulated metasurfaces. *Nano Lett.* **2019**, *19*, 4221–4228.
- (106) Liu, W.; Li, Z.; Cheng, H.; Tang, C.; Li, J.; Zhang, S.; Chen, S.; Tian, J. Metasurface Enabled Wide-Angle Fourier Lens. *Adv. Mater.* **2018**, *30*, 1706368.
- (107) Li, Z.; Liu, W.; Cheng, H.; Choi, D.-Y.; Chen, S.; Tian, J. Spin-selective full-dimensional manipulation of optical waves with chiral mirror. *Adv. Mater.* **2020**, *32*, 1907983.
- (108) Cheng, H.; Wei, X.; Yu, P.; Li, Z.; Liu, Z.; Li, J.; Chen, S.; Tian, J. Integrating polarization conversion and nearly perfect absorption with multifunctional metasurfaces. *Appl. Phys. Lett.* **2017**, *110*, 171903.
- (109) Li, Z.; Liu, W.; Cheng, H.; Chen, S.; Tian, J. Manipulation of the photonic spin Hall effect with high efficiency in gold-nanorod-based metasurfaces. *Adv. Opt. Mater.* **2017**, *5*, 1700413.
- (110) Liu, Z.; Li, Z.; Cheng, H.; Liu, W.; Tang, C.; Gu, C.; Li, J.; Chen, H.-T.; Chen, S.; Tian, J. Single-layer plasmonic metasurface half-wave plates with wavelength-independent polarization conversion angle. *ACS Photonics* **2017**, *4*, 2061–2069.
- (111) Ma, D.; Li, Z.; Zhang, Y.; Liu, W.; Cheng, H.; Chen, S.; Tian, J. Giant spin-selective asymmetric transmission in multipolar-modulated metasurfaces. *Opt. Lett.* **2019**, *44*, 3805–3808.

- (112) Zhao, X.; Li, Z.; Cheng, J.; Liu, W.; Yu, S.; Zhang, Y.; Cheng, H.; Tian, J.; Chen, S. Realization of maximum optical intrinsic chirality with bilayer polyatomic metasurfaces. *Opt. Lett.* **2022**, *47*, 4814–4817.
- (113) Khorasaninejad, M.; Capasso, F. Metalenses: versatile multifunctional photonic components. *Science* **2017**, *358*, eaam8100.
- (114) Arbabi, A.; Arbabi, E.; Kamali, S. M.; Horie, Y.; Han, S.; Faraon, A. Miniature optical planar camera based on a wide-angle metasurface doublet corrected for monochromatic aberrations. *Nat. Commun.* **2016**, *7*, 13682.
- (115) Chen, W. T.; Zhu, A. Y.; Sanjeev, V.; Khorasaninejad, M.; Shi, Z.; Lee, E.; Capasso, F. A broadband achromatic metalens for focusing and imaging in the visible. *Nat. Nanotechnol.* **2018**, *13*, 220–226.
- (116) Wang, Y.; Chen, Q.; Yang, W.; Ji, Z.; Jin, L.; Ma, X.; Song, Q.; Boltasseva, A.; Han, J.; Shalae, V. M.; Xiao, S. High-efficiency broadband achromatic metalens for near-IR biological imaging window. *Nat. Commun.* **2021**, *12*, 5560.
- (117) Jung, C.; Kim, G.; Jeong, M.; Jang, J.; Dong, Z.; Badloe, T.; Yang, J. K.; Rho, J. Metasurface-driven optically variable devices. *Chem. Rev.* **2021**, *121*, 13013–13050.
- (118) Wu, Y.; Chen, Y.; Song, Q.; Xiao, S. Dynamic Structural Colors Based on All-Dielectric Mie Resonators. *Adv. Opt. Mater.* **2021**, *9*, 2002126.
- (119) Yang, B.; Cheng, H.; Chen, S.; Tian, J. Structural colors in metasurfaces: principle, design and applications. *Mater. Chem. Front.* **2019**, *3*, 750–761.
- (120) Hou, X.; Li, F.; Song, Y.; Li, M. Recent progress in responsive structural color. *J. Phys. Chem. Lett.* **2022**, *13*, 2885–2900.
- (121) Yang, B.; Liu, W.; Choi, D.-Y.; Li, Z.; Cheng, H.; Tian, J.; Chen, S. High-performance transmission structural colors generated by hybrid metal-dielectric metasurfaces. *Adv. Opt. Mater.* **2021**, *9*, 2100895.
- (122) Proust, J.; Bedu, F.; Gallas, B.; Ozerov, I.; Bonod, N. All-dielectric colored metasurfaces with silicon Mie resonators. *ACS Nano* **2016**, *10*, 7761–7767.
- (123) Yang, J.-H.; Babicheva, V. E.; Yu, M.-W.; Lu, T.-C.; Lin, T.-R.; Chen, K.-P. Structural colors enabled by lattice resonance on silicon nitride metasurfaces. *ACS Nano* **2020**, *14*, 5678–5685.
- (124) Yang, W.; Xiao, S.; Song, Q.; Liu, Y.; Wu, Y.; Wang, S.; Yu, J.; Han, J.; Tsai, D.-P. All-dielectric metasurface for high-performance structural color. *Nat. Commun.* **2020**, *11*, 1864.
- (125) Huang, Y.; Zhu, J.; Jin, S.; Wu, M.; Chen, X.; Wu, W. Polarization-controlled bifunctional metasurface for structural color printing and beam deflection. *Opt. Lett.* **2020**, *45*, 1707–1710.
- (126) Zhou, M.; Liu, D.; Belling, S. W.; Cheng, H.; Kats, M. A.; Fan, S.; Povinelli, M. L.; Yu, Z. Inverse design of metasurfaces based on coupled-mode theory and adjoint optimization. *ACS Photonics* **2021**, *8*, 2265–2273.
- (127) Zhelyeznyakov, M. V.; Brunton, S.; Majumdar, A. Deep learning to accelerate scatterer-to-field mapping for inverse design of dielectric metasurfaces. *ACS Photonics* **2021**, *8*, 481–488.
- (128) Phan, T.; Sell, D.; Wang, E. W.; Doshay, S.; Edee, K.; Yang, J.; Fan, J. A. High-efficiency, large-area, topology-optimized metasurfaces. *Light Sci. Appl.* **2019**, *8*, 48.
- (129) Liu, W.; Ma, D.; Li, Z.; Cheng, H.; Choi, D.-Y.; Tian, J.; Chen, S. Aberration-corrected three-dimensional positioning with a single-shot metalens array. *Optica* **2020**, *7*, 1706–1713.
- (130) Eliezer, Y.; Qu, G.; Yang, W.; Wang, Y.; Yilmaz, H.; Xiao, S.; Song, Q.; Cao, H. Suppressing meta-holographic artifacts by laser coherence tuning. *Light Sci. Appl.* **2021**, *10*, 104.
- (131) Guo, X.; Zhong, J.; Li, B.; Qi, S.; Li, Y.; Li, P.; Wen, D.; Liu, S.; Wei, B.; Zhao, J. Full-color holographic display and encryption with full-polarization degree of freedom. *Adv. Mater.* **2022**, *34*, 2103192.
- (132) Wen, D.; Cadusch, J. J.; Meng, J.; Crozier, K. B. Multifunctional dielectric metasurfaces consisting of color holograms encoded into color printed images. *Adv. Funct. Mater.* **2020**, *30*, 1906415.
- (133) Mansouree, M.; McClung, A.; Samudrala, S.; Arbabi, A. Large-scale parametrized metasurface design using adjoint optimization. *ACS Photonics* **2021**, *8*, 455–463.
- (134) Nadell, C. C.; Huang, B.; Malof, J. M.; Padilla, W. J. Deep learning for accelerated all-dielectric metasurface design. *Opt. Express* **2019**, *27*, 27523–27535.
- (135) Wiecha, P. R.; Arbouet, A.; Girard, C.; Muskens, O. L. Deep learning in nano-photonics: inverse design and beyond. *Photonics Res.* **2021**, *9*, B182–B200.
- (136) Yang, B.; Ma, D.; Liu, W.; Choi, D.-Y.; Li, Z.; Cheng, H.; Tian, J.; Chen, S. Deep-learning-based colorimetric polarization-angle detection with metasurfaces. *Optica* **2022**, *9*, 217–220.
- (137) Hua, X.; Wang, Y.; Wang, S.; Zou, X.; Zhou, Y.; Li, L.; Yan, F.; Cao, X.; Xiao, S.; Tsai, D. P.; Han, J.; Wang, Z.; Zhu, S. Ultra-compact snapshot spectral light-field imaging. *Nat. Commun.* **2022**, *13*, 2732.
- (138) Fan, S.; Suh, W.; Joannopoulos, J. D. Temporal coupled-mode theory for the Fano resonance in optical resonators. *J. Opt. Soc. Am. A* **2003**, *20*, 569–572.
- (139) Yesilkoy, F.; Arvelo, E. R.; Jahani, Y.; Liu, M.; Tittel, A.; Cevher, V.; Kivshar, Y.; Altug, H. Ultrasensitive hyperspectral imaging and biodetection enabled by dielectric metasurfaces. *Nat. Photonics* **2019**, *13*, 390–396.
- (140) Wang, L.; Kruk, S.; Koshelev, K.; Kravchenko, I.; Luther-Davies, B.; Kivshar, Y. Nonlinear wavefront control with all-dielectric metasurfaces. *Nano Lett.* **2018**, *18*, 3978–3984.
- (141) Bar-David, J.; Levy, U. Nonlinear diffraction in asymmetric dielectric metasurfaces. *Nano Lett.* **2019**, *19*, 1044–1051.
- (142) Liu, B.; Sain, B.; Reineke, B.; Zhao, R.; Meier, C.; Huang, L.; Jiang, Y.; Zentgraf, T. Nonlinear wavefront control by geometric-phase dielectric metasurfaces: influence of mode field and rotational symmetry. *Adv. Opt. Mater.* **2020**, *8*, 1902050.
- (143) Schlickriede, C.; Kruk, S. S.; Wang, L.; Sain, B.; Kivshar, Y.; Zentgraf, T. Nonlinear imaging with all-dielectric metasurfaces. *Nano Lett.* **2020**, *20*, 4370–4376.
- (144) Manzeli, S.; Ovchinnikov, D.; Pasquier, D.; Yazyev, O. V.; Kis, A. 2D transition metal dichalcogenides. *Nat. Rev. Mater.* **2017**, *2*, 17033.
- (145) Caldwell, J. D.; Aharonovich, I.; Cassabois, G.; Edgar, J. H.; Gil, B.; Basov, D. N. Photonics with hexagonal boron nitride. *Nat. Rev. Mater.* **2019**, *4*, 552–567.
- (146) Li, P.; Hu, G.; Dolado, I.; Tymchenko, M.; Qiu, C.-W.; Alfaromozaz, F. J.; Casanova, F.; Hueso, L. E.; Liu, S.; Edgar, J. H.; Vélez, S.; Alù, A.; Hillenbrand, R. Collective near-field coupling and nonlocal phenomena in infrared-phononic metasurfaces for nano-light canalization. *Nat. Commun.* **2020**, *11*, 3663.
- (147) Passler, N. C.; Ni, X.; Hu, G.; Matson, J. R.; Carini, G.; Wolf, M.; Schubert, M.; Alù, A.; Caldwell, J. D.; Folland, T. G.; Paarmann, A. Hyperbolic shear polaritons in low-symmetry crystals. *Nature* **2022**, *602*, 595–600.
- (148) Vaswani, A.; Shazeer, N.; Parmar, N.; Uszkoreit, J.; Jones, L.; Gomez, A. N.; Kaiser, Ł.; Polosukhin, I. Attention is all you need. *Adv. Neural Inf. Process. Syst.* **2017**, *30*, 5998–6008.
- (149) Zhou, J.; Cui, G.; Hu, S.; Zhang, Z.; Yang, C.; Liu, Z.; Wang, L.; Li, C.; Sun, M. Graph neural networks: a review of methods and applications. *AI Open* **2020**, *1*, 57–81.